UNIVERSITY of ROCHESTER

LABORATORY FOR LASER ENERGETICS

January 30, 2014

Ms. Ann Satsangi
Program Manager
High Energy Laboratory Plasmas
Office of Fusion Energy Sciences
U. S. Department of Energy
1000 Independence Avenue, SW
Washington, DC 20585-1290.

Attention: Ms. Ann Satsangi

Subject: Grant DE-FG02-05ER54839

Reference: Final Report, Advanced Concept Exploration for Fast Ignition Science Program

Dear Ms. Satsangi:

Enclosed is a copy of the final report of the project "Advanced Concept Exploration for Fast Ignition Science (ACE-FI) Program", UR Account No 5-23326, for closeout.

Sincerely,

Dr. Wolfgang Theobald
Scientist
Laboratory for Laser Energetics
University of Rochester

UR LLE

250 East River Road
Rochester, New York 14623–1299
(585) 275-5101

ADVANCED CONCEPT EXPLORATION FOR FAST IGNITION SCIENCE PROGRAM

Final Report

by

R.B. STEPHENS,[†] H.M. McLEAN,* W. THEOBALD, K. AKLI,[‡] F.N. BEG,[¶] Y. SENTOKU,[§] D. SCHUMACHER,[‡] and M.S. WEI[†]

[†]General Atomics, San Diego, California.
***Lawrence Livermore National Laboratory, Livermore, California.**
[‡]Ohio State University, Columbus, Ohio.
[¶]University of California San Diego, La Jolla, California.
[§]University of Nevada, Reno, Nevada.

Principal Investigator: **Dr. Wolfgang Theobald**

Street Address/City/State/Zip: **518 Hylan Building, Rochester NY, 14623-0140**

Postal Address: **Laboratory for Laser-Energetics, University of Rochester, 250 East River Rd., Rochester NY, 14623-1299**

Telephone Number: **(585) 273-2628**

Email: **wthe@lle.rochester.edu**

DOE/Office of Science Program Office: **Office of Fusion Energy Sciences**

DOE Grant Number**: DE-FG02-05ER54839**

UR Account No: **5-23326**

Submission Date: January 31, 2014

Final Project Report

"Advanced Concept Exploration For Fast Ignition Science Program"

Table of Contents

1. Executive Summary

The Fast Ignition (FI) Concept for Inertial Confinement Fusion has the potential to provide a significant advance in the technical attractiveness of Inertial Fusion Energy (IFE) reactors. FI differs from conventional "central hot spot" (CHS) target ignition by decoupling compression from heating: using the laser (or heavy ion beam or Z pinch) drive pulse (10's of ns) to create a dense fuel and a second, much shorter (~10 ps) high intensity pulse to ignite a small region of it. There are two major physics issues concerning this concept; controlling the laser-induced generation of large electron currents and their propagation through high density plasmas.

This project has addressed these two significant scientific issues in Relativistic High Energy Density (RHED) physics. Learning to control relativistic laser matter interaction (and the limits and potential thereof) will enable a wide range of applications. While these physics issues are of specific interest to inertial fusion energy science, they are also important for a wide range of other HED phenomena, including high energy ion beam generation, isochoric heating of materials, and the development of high brightness x-ray sources. Generating, controlling, and understanding the extreme conditions needed to advance this science has proved to be challenging: Our studies have pushed the boundaries of physics understanding and are at the very limits of experimental, diagnostic, and simulation capabilities in high energy density laboratory physics (HEDLP). Our research strategy has been based on pursuing the fundamental physics underlying the Fast Ignition (FI) concept.

We have performed comprehensive study of electron generation and transport in fast-ignition targets with experiments, theory, and numerical modeling. A major issue is that the electrons produced in these experiments cannot be measured directly—only effects due to their transport. We focused mainly on x-ray continuum photons from bremsstrahlung and x-ray line radiation from *K*-shell fluorescence. Integrated experiments, which combine target compression with short-pulse laser heating, yield additional information on target heating efficiency. This indirect way of studying the underlying behavior of the electrons must be validated with computational modeling to understand the physics and improve the design.

This program execution required a large, well-organized team and it was managed by a joint Collaboration between General Atomics (GA), Lawrence Livermore National Laboratory (LLNL), and the Laboratory for Laser Energetics (LLE). The Collaboration was formed 8 years ago to understand the physics issues of the Fast Ignition concept, building on the strengths of each partner. GA fulfills its responsibilities jointly with the University of California, San Diego (UCSD), The Ohio State University (OSU) and the University of Nevada at Reno (UNR). Since RHED physics is pursued vigorously in many countries, international researchers have been an important part of our efforts to make progress. The division of responsibility was as follows: (1) LLE had primary leadership for channeling studies and the integrated energy transfer, (2) LLNL led the development of measurement methods, analysis, and deployment of diagnostics, and (3) GA together with UCSD, OSU and UNR studied the detailed energy-transfer physics. The experimental program was carried out using the Titan laser at the Jupiter Laser Facility at LLNL, the OMEGA and OMEGA EP lasers at LLE and the Texas Petawatt laser (TPW) at UT Austin. Modeling has been pursued on large computing facilities at LLNL, OSU, and UCSD using codes developed (by us and others) within the HEDLP program, commercial codes, and by leveraging existing supercomputer codes developed by the NNSA ICF program.

This Consortium brought together all the components—resources, facilities, and personnel—necessary to accomplish its aggressive goals. The ACE Program has been strongly collaborative, taking advantage of the expertise of the participating institutions to provide a research effort that is far greater than the sum of its parts. The results of this work have firmly strengthened the scientific foundation from which the viability of FI and other applications can be evaluated. Program execution has also led to improved diagnostics for probing dense, hot plasmas, detailed understanding of high-current, relativistic electron energy generation and transport across boundaries and into dense plasmas, and greatly enhanced predictive modeling capabilities. One important aspect of this program was the involvement and training of young scientists including postdoctoral fellows and graduate students. During the entire 8 years of FI and ACE project period since 2005, more than fifteen graduate students completed their doctoral dissertations including three from OSU and two from UCSD in last three years. This project generated an impressive forty articles in high quality journals including nine (including two under review) in Physical Review Letters during the last funding period since 2011.

2. Background

Many groups around the world have studied the basic Fast Ignition (FI) concept since it was first proposed [Tabak94, Basov92]. The concept is different from conventional central hot spot (CHS) in the sense that compression and ignition phases are separate. It was immediately recognized as an attractive concept that was compatible with any fuel compression driver (*i.e.* laser, *Z*-pinch, and ion beams) and had the potential for higher gains and smaller driver energy requirements than the CHS approach. The initial concept is shown schematically in Fig. 1. Here the fuel is compressed by an external driver; subsequently, a powerful precursor laser pulse of about 10^{-10}s duration is focused to a small spot on the compressed fuel to expel plasma radially by the ponderomotive force creating a channel through the ~1 mm of coronal plasma up to the critical density, the location of which is pushed back by light pressure in a hole-boring process. A subsequent ignitor pulse is then propagated through the channel to the critical surface where a stream of energetic electrons (several MeV) is produced. The energy distribution of the laser-generated electrons should have a range matching the ρR~0.6g/cm^2 of the ignition hotspot in the compressed core [Li04], with the result that a small fraction of the core is elevated to ignition temperatures.

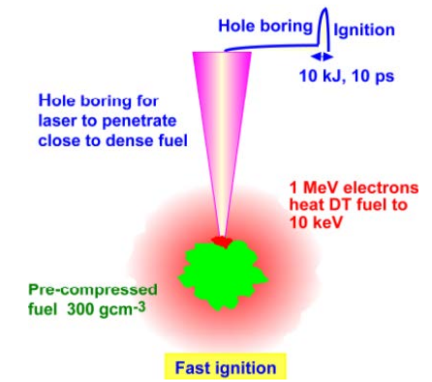

Fig. 1: Schematic of the channeling and hole-boring concept first proposed for fast ignition.

Early research on laser-induced plasma channels, and propagation of powerful pulses in those channels, showed that there were many complications, thus motivating an alternative design using a hollow Au cone inserted in the spherical shell [Hatchett00, Kodama02] as illustrated in Fig. 2. In this design, the fuel implosion produces dense plasma at the tip of the cone, while the hollow cone permits the short-pulse ignition laser to be transported inside it without interference, and enables the generation of hot electrons at its tip, very close to the dense plasma.

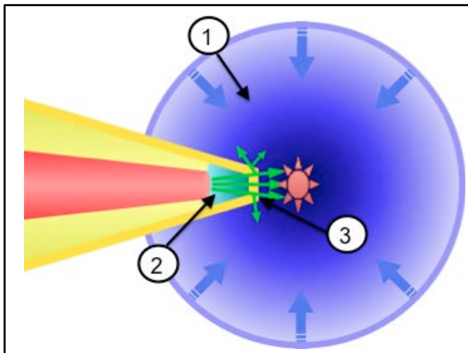

Fig. 2: The cone-guided implosion concept sequence: (1) The DT fuel is compressed to high ρ, ρR around cone tip using a 0.5 − 1 MJ, 20 ns compression drive, (2) a 100-200 kJ, 20 ps laser generates 1-3 MeV electrons, and (3) Those electrons travel out of the cone and through overlaying fuel layers to deposit their energy in the dense core.

Over the last 12 years investigating the fast ignition concept has proved to be challenging. Injection of the ignition energy involves enough power- and energy-density (I_{Laser}>10^{20}Wcm^{-2}, pressure>Gbar, magnetic field *B*>100MGauss, electric field *E*>10^{12}V/m) and large numbers of relativistic particles ($kT_{electron}$>MeV, $I_{electron}$>1GAmp) to enter a new regime—a relativistic high energy density (RHED) plasma—whose properties vary substantially from their less energetic brethren. Experimental access to this regime in a limited way began with operation of the LLNL Nova PW followed, after its retirement, by a number of other lasers. None of these were capable of providing an RHED environment for research in the FI relevant regime until the recent availability of PW, high energy (>kJ), longer pulse (~10 ps) facilities (OMEGA, OMEGA EP at LLE; LFEX at ILE in Japan). Because of considerable progress over the last few years in understanding the issues critical to the fast ignition concept and advances in predictive modeling capabilities, we have been well positioned to perform expanded experimental efforts on these newer facilities. Our goal was to understand the interplay of forces involved with the creation, injection, and transport of relativistic electrons into HED plasmas. Such scientifically rich understanding with the benchmarked modeling codes has led to our improved capability to extrapolate to FI ignition conditions and evaluate the FI concept.

Section 3 details our progress and accomplishments over the last few years of our Advanced Concept Exploration (ACE) program (started Aug. 2005). Section 4 summarizes the achievements and impacts of the ACE program. A list of PhD theses and scientific papers published during the last three years are detailed in Section 5.

3. Progress and Accomplishments

This section describes the work to date of the Fast Ignition Advanced Concept Exploration (ACE) consortium. The program concentrated on the problem common to all electron-based FI schemes—*the physics of the ignitor mechanism*—and interacted closely with other FI-related, DOE-funded programs such as the Fast Ignition-High Energy Density Science (FI-HEDS) project at LLNL and the Fusion Science Center for Extreme States of Matter (FSC) at the University of Rochester. Our activity had three thrust areas:

- Understanding of the production and distribution of fast electrons resulting from FI-relevant laser-plasma interactions (LPI) and its dependence on laser prepulse (pre-plasmas density scalelength) and laser pulse length (from typical sub-ps to 10 ps)
- Investigating the subsequent fast electron transport in solid and through hot (FI-relevant) plasmas.
- Conducting and understanding integrated core-heating experiments by comparison to simulations.

The program included development of:

- Diagnostics and experimental platforms to facilitate the characterization of fast electron beams, energy transport and imploded plasmas targets
- Improved codes with added physics models that can better simulate the experiments on the FI-relevant temporal and spatial scales

The ACE collaboration (including its predecessor, the "FI Exploration") over the past 8 years has endeavored, with good success, to build a firm scientific foundation for describing fast electron generation and subsequent transport. We have overseen an ever-increasing sophistication of computational tools and experimental techniques, and can often now approach many aspects of the science in a basic, "predict & test" fashion. The progress detailed below shows that our FI-focused strategy, by virtue of its emphasis on the underlying fundamental science, has been effective in addressing the FI specific issues as well as other deeply scientific questions that are present and important in virtually all HEDP research.

The accomplishments on the three thrust areas are detailed below. References are listed in the bibliography in Section 6. Published works that have a significant component of ACE funding are shown in **bold** typeface.

3.1. Fast Electron Source

The principal short-pulse laser interaction with a target occurs near the critical plasma density surface. The interaction is highly dynamic; the position/shape of that surface, and of the overlying plasma, co-evolves with the distribution of laser intensity in a complex manner throughout the pulse. Target material starts as a cold solid, and ends as hot plasma, evolving through several material regimes that are not well understood in static, equilibrium conditions, much less during rapid transients. The science of the interaction is supremely challenging, pushing the limits of experimental and computer modeling capabilities. Our focus in this area remains the development of a complete FI-relevant microscopic description of the laser plasma interaction and characterization of the resulting temporal-, spatial-, and angular-distributions of the electron particle and energy flux. Full predictive capability over a wide range of conditions is an ultimate goal, a Grand Challenge that will likely need significant effort in concert with the larger HEDLP community.

3.1.1. Fast electron spectrum and conversion efficiency

The main objectives of the study are to understand LPI produced fast electron source spectrum, laser-to-electron energy conversation and evaluate the effects of laser intensity, preplasma and laser pulse length via both numerical simulations and experiments using a variety of high intensity lasers covering from sub-ps, 100-J level intermediate facilities to the 10ps, >1kJ energy OMEGA EP laser.

The ponderomotive force of high-intensity laser pulse has been shown to compress plasma near the critical surface. 1-D PIC and hybrid-PIC simulations [Chrisman08, Kemp08] show the result as a step-function: plasma density greater than critical is compressed while that just below critical spreads out, creating a plateau in the density just before a steep increase. Detailed 1-D analysis of this structure by Paradkar et al. [**Paradkar11**] shows that the sub-ps short laser creates a potential well within this plateau within which the electrons are trapped and heated (see Fig. 3). Motion of the electrons within the well is stochastic, with the occasional electron gaining much more than the laser ponderomotive energy; this motion facilitates the characteristic hot tail in the electron spectrum. Systematic study of different pre-formed plasma scale lengths and laser intensities show a mean energy increase with plasma scale-length.

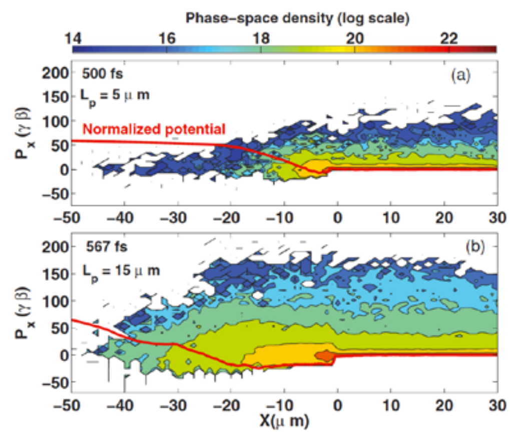

Fig. 3: Comparison of phase-space plots for (a) 5μm and (b) 15μm preformed plasma scale lengths (laser intensity= 10^{20}W/cm^2). Note the extension of the phase-space mixing region (0 to −45μm) for the case of 15μm preformed plasma with higher energies compared to 5μm preplasma. Also, the electrostatic potential well developed in the preformed plasma due to the electron heating is wider for long-scale-length preformed plasma. [**Paradkar11**, Fig. 6].

Simulations [**Sorokovikova12**] using the LSP code [Welch06] have been further extended using FI relevant high intensity laser pulse at a time scale of multiple picoseconds and the laser energy scale of kilojoules. We have found that fast electron mean energy and laser-electron conversion efficiency increase with laser pulse duration from 1 to 10 picoseconds as shown in Fig. 4, which is different from the previously studied dynamics in the sub-ps regime. Fast electron energy spectra in all cases show two temperature components. The slope temperature of the lower-energy component independent of the laser pulse length in 1-10 ps range is about 3.9 MeV, agreeing well with the ponderomotive scaling. However, the slope temperature of the high-energy component (marked on Fig. 4a) is much higher and also increases with the pulse length. It is found that a step-function-like density profile of preplasma (Fig. 5a-d) is formed, consisting of a long flat shelf at near critical density ($0.1n_c < n_e < n_c$) and a steep critical density surface jumping from n_c to γn_c, due to the hydrodynamic responses of plasma in picoseconds including thermal expansion by laser heating and density steepening by laser ponderomotive pressure. This results in a large and broad electrostatic potential well that traps and enhances fast electron acceleration to a much higher energy. It is seen that the longer pulse durations enhance both the density steepening and preplasma expansion effects. Both the heights of the sharp critical surface and the length of the low-density flat shelf significantly increase by extending the pulse durations from 1 to 10ps. And this correspondingly results in forming the wider and deeper electrostatic potential well to enhance the electron acceleration, as shown in

Fig. 5(e). It has also been verified that the low-energy electrons (< 4 MeV) originates from the steep

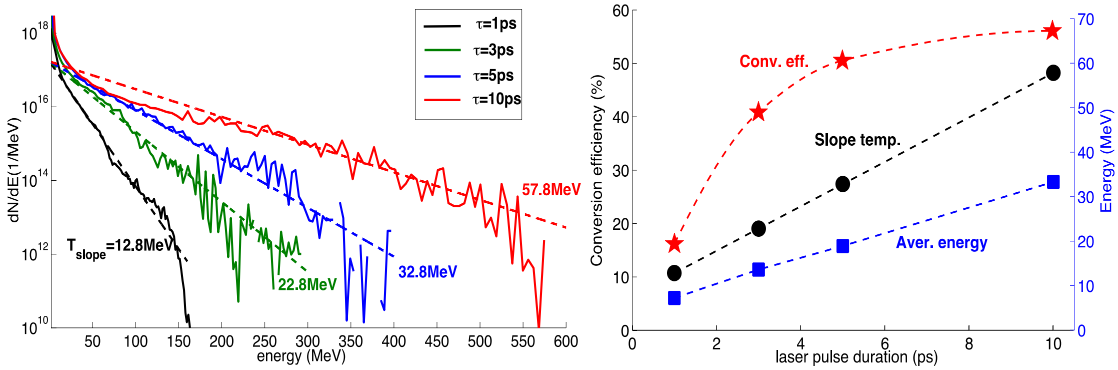

Fig. 4: Time-integrated energy spectra of hot electrons entering into the solid density target for different laser pulse durations; b) the laser-electron conversion efficiency, th slope temperature for the high-energy component of the spectrum, and average energies of hot electrons varying with different laser pulse durations. Simulations are in 1D with peak laser intensity at 10^{20}W/cm^2 and a 10 μm preplasma scalelength.

critical surface region $(n_c < n_e < \gamma n_c)$ directly accelerated by ponderomotive pressure and **j×B** heating within a skin depth, while the high-energy ones comes from the enhanced acceleration in the potential well at the long flat shelf region $(0.1n_c < n_e < n_c)$.

Another important finding is that the electron acceleration dynamics becomes less sensitive to the initial preplasma density scale length (tested with 5 – 15 μm scalelength) if the laser pulse has several-picosecond duration, because the plasma density profiles are fully self-organized due to the hydrodynamic thermal expansion driven by the same laser conditions. A manuscript has been prepared to report these new findings for fast electron production with up to 10 ps pulse duration [**Sorokovikova13**].

It should be pointed out that the multi-dimensional effects of laser-plasma interactions such as self-focusing, filamentation, magnetic field generation are excluded in the present 1D studies. Therefore our

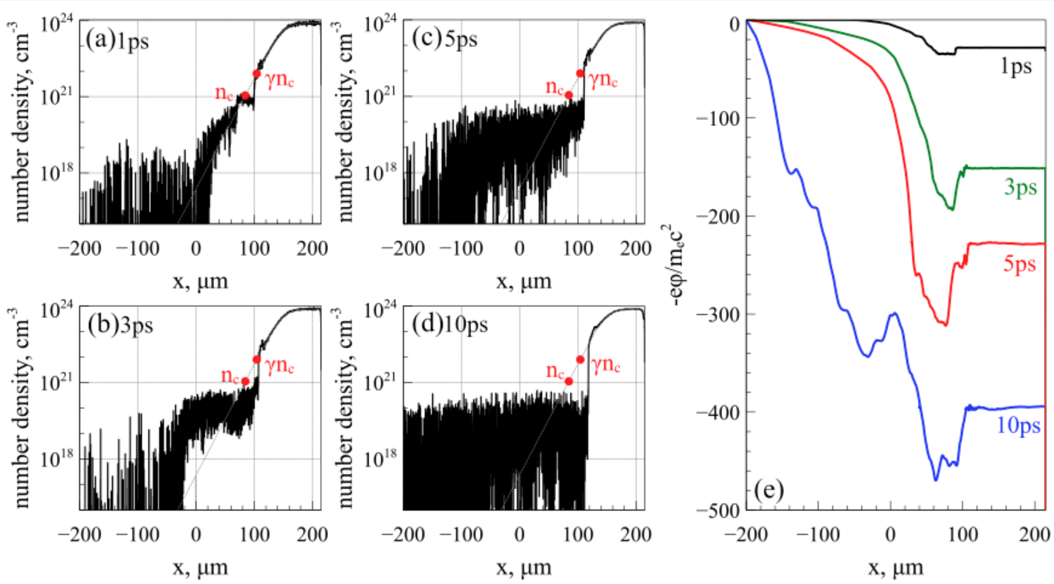

Fig. 5: (a) Fig. 4 (a)-(d) the electron density profiles at the laser field peak time for intense laser interaction solid targets with pulse duration respectively of T=1, 3, 5, 10 ps. n_c and γn_c marks the initial critical and relativistic critical density positions. (e) shows the corresponding electrostatic potentials respectively.

1D description oversimplifies the dynamics of either the sharp critical surface or the near-critical long flat shelf. Plasma expansion in additional degrees of freedom in the second transverse dimension may cause the flat shelf to be less obvious than in 1D and strong magnetic field may be generated near the critical region, stopping fast electrons entering into solid target. Two-dimensional PIC simulations are underway.

In this project, we also experimentally investigated the relativistic electron beam properties. Chen et al., [**Chen09**] investigated the electron spectra and conversion efficiency by measuring bremsstrahlung x-rays from planar targets at the Titan laser in Lawrence Livermore National Laboratory. The laser-to-electron conversion efficiencies of 20-40% above I~10^{19} W/cm^2 were inferred by fitting with Monte Carlo calculations using the ITS code [Halbleib92] assuming two temperature electron spectra and classical ejection angle. A synthetic electron distribution was constructed from a ponderomotive scaling [Wilks92] applying to the measured focal spot. The result was consistent with the 2-T_e parameterization when the scaling factor is reduced to 75%. The large uncertainty attributed to the divergence model in the analysis was studied by applying various ejection angles [**Westover11**]. The bremsstrahlung data were modeled with ITS code using the synthetic electron spectra and varying divergence angle model (classical, 15, 75°, and PIC modeling predicted angle). The conversion efficiencies in the laser energy between 15 and 150J were inferred to be 20% (classical) - 60% (75°) (Fig. 6). The effect of fields in these analyses was neglected.

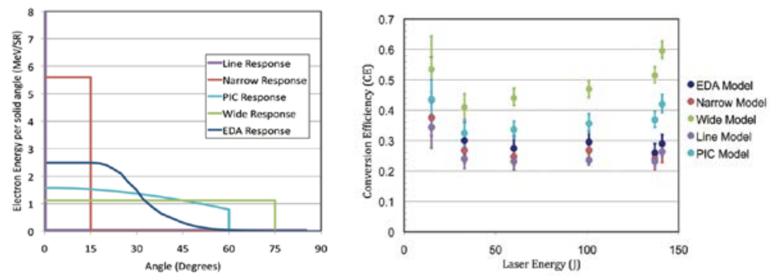

Fig. 6: (a) Different models of electron angular distribution are compared. The Line model represents a zero-divergence beam; the Narrow a 15° divergence; the Wide a 75° divergence beam, and the other models have more complex profiles. (b) The conversion efficiency of laser energy into electrons, as calculated using various models for the angular distribution of electrons. The inferred conversion efficiency is higher when a wider beam of electrons is injected. The Wide and Line divergence models should be considered maximum and minimum conversion efficiencies determined by this technique. [**Westover11**, Fig. 5, 9].

We have done further experiments at the Titan laser where multiple bremsstrahlung spectrometers were fielded at three different angles (0°, 28° and 66°) relative to the target rear normal direction to constrain the divergence angle. A 2-D multi-stage simulation model incorporating realistic laser conditions and a fully resolved electron distribution handoff has been developed and compared to angularly and spectrally resolved Bremsstrahlung measurements from high-Z planar targets. This method is more detailed and precise than the previous analyses of similar data. LPI and the resultant electron source modeled using the 2D PIC code PSC [Kemp10] with the experimentally measured laser intensity distribution showed that there are two components to the fast electron distribution: (i) a symmetric, broad, forward directed component and (ii) an asymmetric high-energy component directed away from the laser axis. They are spatially separated. The total conversion efficiency into forward going fast electrons is 68%–70%. The angular distribution of the symmetric component is flat across all energies at both intensities, with $\Delta\theta$~31°, which is defined as the average absolute deviation about the mean (about 0° for the symmetric component, about the mean direction for the asymmetric component). The asymmetric component is narrower: $\Delta\theta$~20°. Taking the PIC predicted electron source distribution, transport simulations were performed with the hybrid-PIC code ZUMA [Larson10] including the field effects. Simulated Bremsstrahlung signals are obtained by summing the Bremsstrahlung emission from the ZUMA transport simulations, applying cold matter opacity corrections and folding the spectrum with the spectrometer response function [**Chen13**]. As shown in Fig. 7, the simulated data matches well with the measured results.

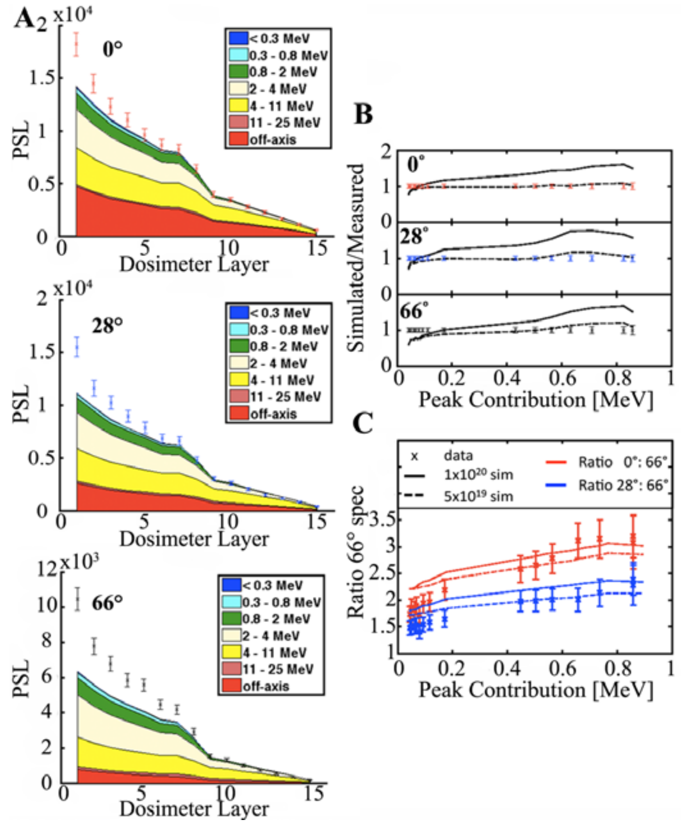

Fig. 7: (a) Bremsstrahlung signals from the 5×10^{19} W/cm^2 simulation are broken down by original electron energy and plotted against measurements. (b) Simulated signals are normalized to the respective measured signals to visualize spectrum temperature and coupling efficiency for the two simulations, baseline (1×10^{20} W/cm^2, solid) and half intensity (5×10^{19} W/cm^2, dashed). (c) Simulated and measured ratios between different spectrometers are plotted for visualization of the electron divergence for the two simulations. Solid lines and dashed lines represent the nominal and half intensity cases, respectively. Red and blue represent the ratios of 0°: 66° and 28° : 66°, respectively. [**Chen13**, Fig. 5]

To understand time evolution of the LPI dynamics from sub-ps to 10 ps pulse duration and the role of preplasma, we have performed a series of experiments [**Wei12, Wei13a,b, Peebles13**] at the OMEGA EP laser systematically varying the laser pulse-length (from 0.7 ps to 10 ps) and corresponding energy (from 100-150 J to 1500 J respectively) to keep the laser intensity the same, first with the low contrast OMEGA EP pulse with prepulse energy about 100 mJ, followed by a very recent campaign using the improved high contrast OMEGA EP pulse with prepulse energy (< 1 mJ). Multi-layered solid foil targets used in this study are composed of an Al substrate, a Cu fluorescence diagnostic layer buried ~125 µm from the front surface and a thick conductive CH back layer to minimize fast electron refluxing. To better characterize the LPI generated fast electron source characteristics, we also built and implemented two fixed-port high-energy bremsstrahlung MeV x-ray spectrometers described in [**Chen09, Chen13**] onto the OMEGA EP chamber. ITS Monte Carlo modeling analysis of the measured bremsstrahlung signal assuming a one temperature exponential energy distribution for fast electrons with fit best to a divergence angle of 60±5° (for both the low and high contrast LPI cases) suggests an increasing trend for the inferred fast electron temperature with laser pulse length varied from 0.7 to 10 ps (see Fig. 8). This is the case for the LPI with both the low and high contrast laser pulses. The inferred conversion efficiency from the laser to fast electrons transported into the solid target is insensitive to laser pulse length for a given laser pulse contrast. When comparing the inferred laser-to-electron conversion efficiency and fast electron temperature with the low and high contrast pulses, the values for both parameters seem to be slightly higher with the high contrast EP pulse which is consistent with the trends observed in PIC simulations mentioned above. Further analysis using the hybrid-PIC transport code ZUMA code is ongoing to include the field effects.

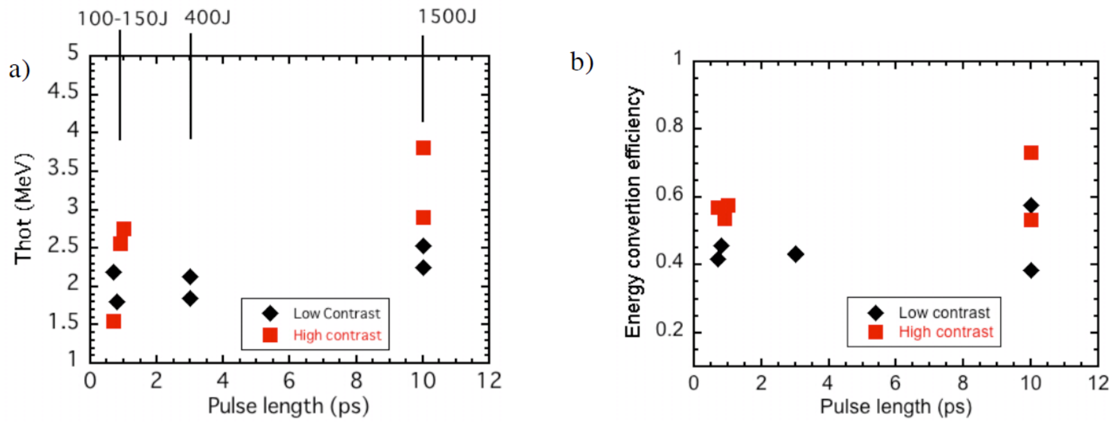

Fig. 8: a) Inferred fast electron slope temperature (assume an exponential energy spectrum with one slope) and b) laser-to-electron conversion efficiency as a function of laser pulse length with both low and high contrast EP beam from the ITS Monte Carlo modeling. Corresponding laser energy for each pulse length is marked on Fig. (a).

We have also used LSP simulations to understand the relationship between the experimentally measured electron spectra by the magnetic spectrometer and the intrinsic LPI produced electron energy distributions by examining the effect of propagation through the target of an initial electron distribution injected near the front surface of the target [**Link11**]. We found that the electron energy spectrum becomes divided into two regions: a low temperature electron distribution (as defined by the exponential fall-off with energy) and a high temperature distribution. The former is determined by energy exchanged with rear-surface ions via target normal sheath acceleration and provides no direct information about the LPI. Since this low temperature region can extend up to several MeV, including the critical energy range for Fast Ignition of 1-3 MeV, this is an important finding. The high energy region experiences significant energy modification due to target charging, but typically in a fashion that does not change the hot electron temperature. We note that two-temperature fits are common of the ponderomotive region of the electron spectrum, but out results indicate that the physical basis for the two temperatures is quite different.

3.1.2. Fast electron divergence study and LSP simulation analysis

The objective is to perform detail experimental and simulation study of fast electron divergence and its dependence on preplasma scale length and laser intensity.

The focus has been on understanding intense laser-plasma interactions and their measurement using $K\alpha$ based diagnostics. Our effort has been focused on the analysis of the data collected using the Titan laser (LLNL) and the Texas Petawatt Laser (UT) using simulations performed with the PIC code LSP and the Monte Carlo code ITS. We have examined $K\alpha$ image formation and its use in determining electron angular distributions [**Ovchinnikov11a**, **Ovchinnikov11b**]. We found that $K\alpha$ images are relatively insensitive to the details of the LPI including many aspects of laser propagation through mid-scale pre-plasmas such as filamentation. Such images are sensitive to the subsequent propagation of the LPI generated hot electrons through the target, including refluxing and, for $K\alpha$ images near the target front surface (ie. not buried too deeply), to the temperature varying conductivity of the target. Laser generated quasi-static magnetic fields near the critical surface also play a key role. Because of these varying effects, the images themselves may not be indicative of the true fast electron divergence. However, accounting for these effects permits good match between experiment and simulation (Fig. 9). We find that targets for which back surface refluxing is controlled using “get-lost-layers” and which have large transverse extent

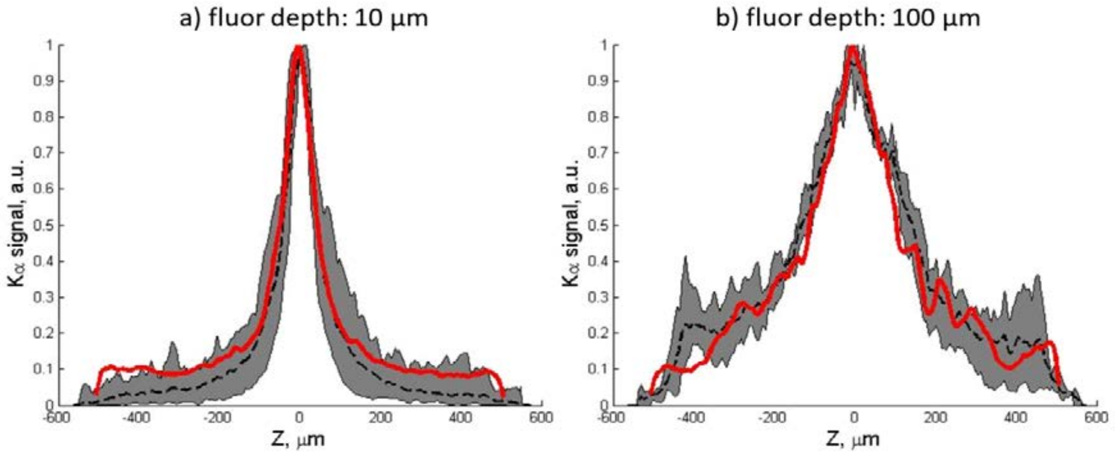

Fig. 9: Experimental (grey – showing range of data) and modeled (red) Kα images for two copper fluor depths from reference [**Ovchinnikov11a**]. The pre-plasma scale length was the only adjustable parameter in the simulation with a value of 3.8 µm being used. The simulation indicates that the distance from the critical surface to the target front surface is the key factor and the shape of the pre-plasma profile itself is not critical.

to control side-refluxing can provide a good measure of the intrinsic hot electron divergence, which is generally found to be large with full angles of ~60^{o} for Titan like excitation. Finally, we also found that the Kα image background provides an excellent diagnostic of the operation of rear-surface get-lost-layers.

We performed a series of full-scale, 2D3V numerical simulations on the effects of pre-plasma scale length and laser intensity on the hot electron (~ 1 MeV) divergence angle using LSP. We examined intensities in the range from 10^{18} to 10^{21} W/cm^2 and exponential preplasma scale lengths from 1 to 5 μm [**Ovchinnikov13**], a range covering many recent experimental studies in this area. Our results indicate that the hot electron divergence angle increases approximately linearly with the preplasma scale length for a fixed laser intensity whereas, for a fixed scale length, the laser intensity has only modest impact on the divergence angle over the range considered [Fig. 10]. These findings have important implications for the

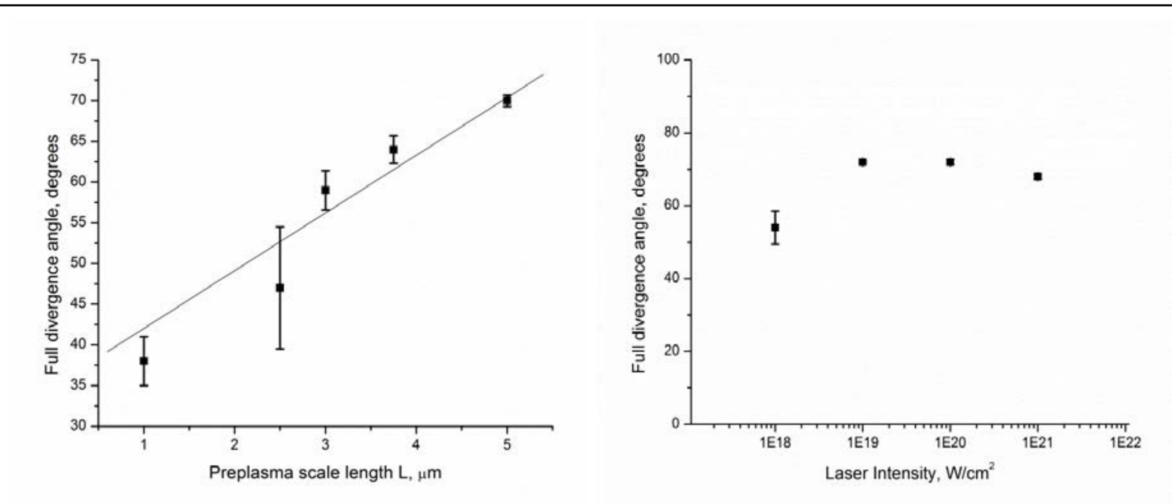

Fig. 10: (left) Electron beam divergence vs. pre-plasma scale length. Each point and error bar is derived from the growth of the electron spot size at three different depths. The black curve is a linear fit. Divergence angle increases 7.0°±0.6^{o} for each 1 μm increase of scale length L. (right) Electron beam divergence vs. laser intensity. Error bars on the graph are from the fitting errors.

interpretation of experimental results especially if, for example, the intensity dependence studies do not maintain a constant preplasma profile as the intensity of the main pulse is varied. The simulations were first benchmarked using recent Kα images collected at the Titan laser facility.

We examined the time-dependence of Kα image formation using simulations benchmarked by the Texas Petawatt laser (TPW, UT) [**Akli12a**]. The laser delivered 50 J of energy in a 250 fs (FWHM) pulse with a peak laser intensity of 1.2 x 10^{20} W/cm^2. The time integrated electron beam full divergence was found to be 60^o +/- 5^o. Numerical simulations yielded time-integrated Kα images in good agreement with experiment. However, the simulations also found that the time-resolved divergence varied significantly, with the initial beam divergence 30^o and then increasing monotonically with time (Fig. 11). We find that a substantial fraction of the laser energy (~7%) is transported up to 100 μm with a divergence of 32^o. The time variation of LPI generated hot electron distributions is of fundamental importance and crucial for applications using these electrons.

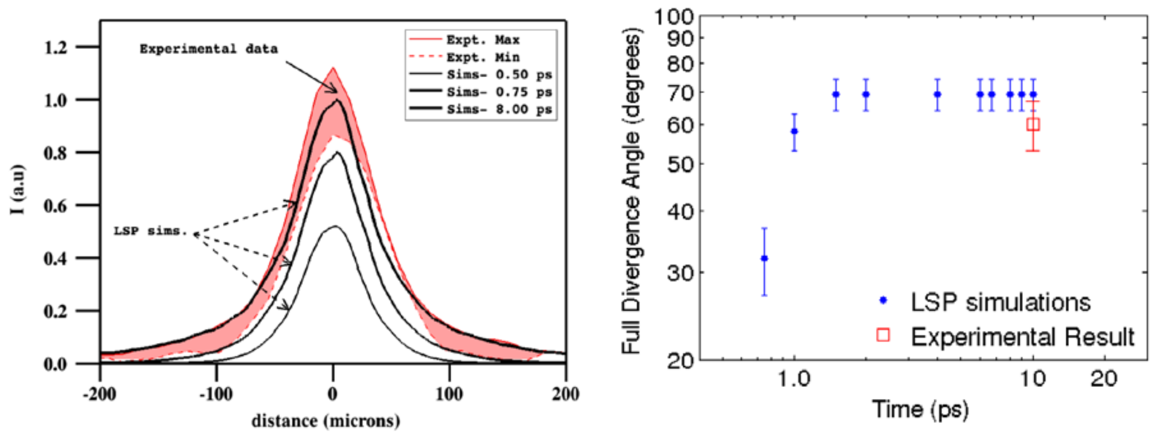

Fig. 11: (left) Time evolution of Kα emission at a depth of 15 μm into the target. The red band represents the range of experimental data using time integrating detectors. The black curves are profiles obtained from simulations at various times, as indicated. (right) Time-dependent divergence from LSP simulations (blue) and time-integrated experimental measurements (red).

3.1.3. Cone material effects on Energy Coupling

The objective is to detail effects of pointing and interface material on electrons' generation and propagation out of a cone tip.

Two Titan campaigns (E~150 J, τ~0.7ps) were conducted to characterize LPI-generated fast electrons at both planar and buried cone surfaces. The x-ray fluorescence from fast electrons transiting the buried Cu fluor layers in the target was imaged with a 2-D $K\alpha$ imager, and the hard x-ray bremsstrahlung was recorded on spectrometers at multiple angles. Energy coupling of laser light to hot electrons was seen to be as much as 2X larger for buried cones compared to flat targets, but with an increased electron fluorescence spot size, the effect varying with cone material (Fig. 12). Data suggest that the observed spot size and the inferred spatial distribution are sensitive functions of preformed plasma scale-length. It is known that the pre-plasma modifies the laser plasma interaction [**MacPhee10**], and even with the low intrinsic prepulse (E_{pre}~10mJ) of the Titan CPA beam, the cones in our experiments were prefilled with plasma.

The difference in the observed large angular spread from the buried Au cones can be attributed to the more extended preplasma (Fig. 13) produced inside the Au cone target by the laser prepulse, which was modeled by the 2D radiation hydrodynamics code HYDRA [Marinak98] using the experimentally measured prepulse profile. HYDRA-simulated preplasma profiles are fed into PIC simulations to study LPI and fast electron source characteristics using the collisional PIC code PICLS [Sentoku08, **Mishra13**] that includes dynamic ionization (due to field and collisions) and radiation cooling. A Gaussian laser pulse (1μm wavelength, 726 fs, 10 μm spot, I_{peak}~9×10^{19} W/cm^2) is normally incident on the target front surface. Fig. 5 shows the simulated electron energy density plots at 500 fs for three different cases, i.e., a) planar Al target, b) buried Al cone, and c) buried Al cone with 10 μm thick Au tip. For all these cases, the corresponding preplasma profiles were included atop of the solid density plasmas (marked as the white dash lines in Fig. 14). It can be clearly seen that due to the extended preplasma inside the buried cones, fast electrons are generated from a large volume of preplasma during the laser pulse propagation. The laser beam undergoes self-focusing and hole boring into the relativistic corrected critical density region and is also subject to hosing instability. The resultant fast electrons enter into the solid density targets with a large angular spread, most prominent in the buried Au cone case [Fig. 14(c)] compared to that in the Al planar target [Fig. 14(a)], while the angular spread in the buried Al cone [Fig. 14(b)] is somewhere in between. The simulation results agree qualitatively with the observed differences in the Cu Kα spot sizes in Fig. 12. These results were reported as invited presentations at the 2011 EPS Plasma Physics Conference [**Wei11**] and the 2012 IAEA FEC meeting [**Wei12**].

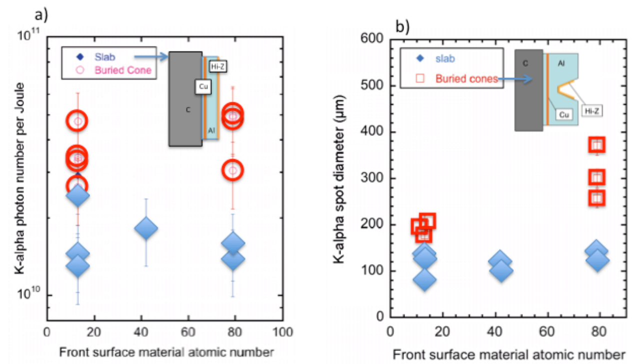

Fig. 12: a) Normalized fluorescence intensity, and b) fluorescence spot diameter from Cu layers buried 100 μm below a front surface hi-Z layer that is either planar or conical, as shown in the insets. The targets were mounted on a thick carbon layer that insured the fluorescence would not be modified by refluxing electrons.

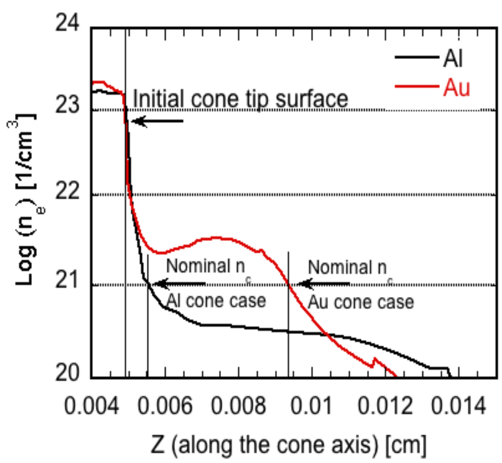

Fig. 13: Axial lineout of the HYDRA-simulated preplasma density profiles prior to the arrival of the main pulse for the Au and Al cones with the measured prepulse energy of 17 mJ in 2.3 ns.

3.1.4. Detailed studies of preplasma effects on energy coupling and demonstration of high energy coupling using the high contrast laser pulses using the cone-wire targets

The objective is to understand the detail effects of pre-plasmas on fast electrons propagating out of a cone tip and optimization energy coupling using high-contrast laser pulses

Our results reveal that even the small pre-pulse levels present at the Titan laser facility (E_{pre}~10mJ, ~ 2.5 ns for E_{pulse}~150J, 0.7 ps), cause a noticeable effect on the amount of energy coupled into a cone-wire. A systematic study found significant further reduction (one order of magnitude) occurs with the increase of prepulse energy to 1 J (with correspondingly larger pre-plasma scale length) [**Ma12**]. This was also confirmed by the latest results on the 10 ps, 1 kJ class OMEGA EP laser [**Yabuuchi13a**] using identical

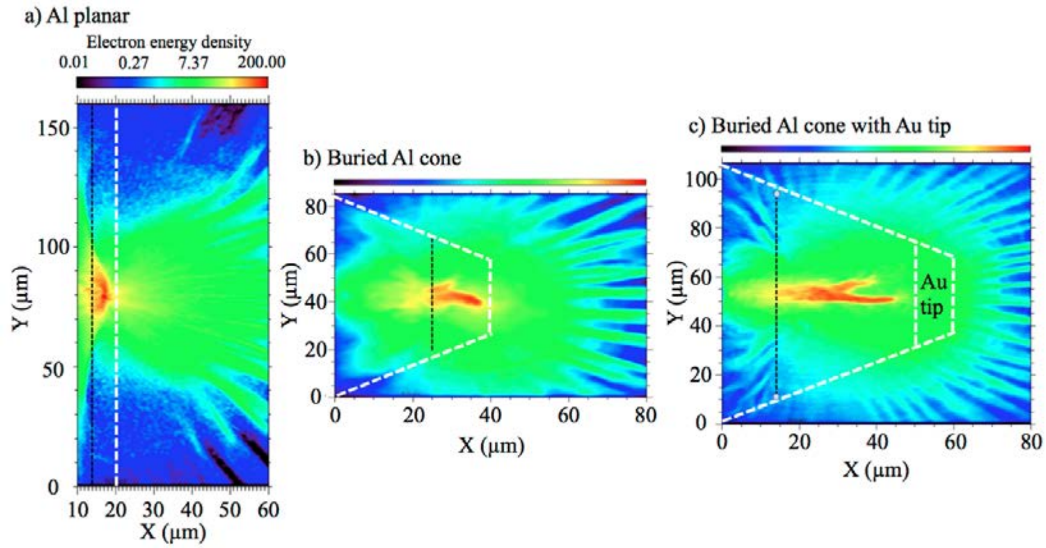

Fig. 14. Electron energy density contour plots at 500 fs from the PICLS simulations for (a) Al planar target, (b) buried Al cone, and c) buried Al cone with Au tip. The white dash line in (a) marks the interface between the preplasma and the solid density target and those in (b) and (c) show the inner cone wall and tip. The black dash line in each figure indicates the initial location of the classical critical density for 1 μm wavelength laser.

cone-wire targets. The observed Cu Kα coupling efficiency at the OMEGA EP experiment was ~ 5x lower than the average value at Titan with the intrinsic prepulse, which can be attributed to the large prepulse (E_{pre}~ 500 mJ) in the OMEGA EP experiments. The preplasma scale length was simulated using the 2D HYDRA code (Marinak98] and was estimated to be 35μm near the critical density region, which was about 130μm from the initial cone tip. 2D PICLS simulations which include dynamics field and collisional ionization, relativistic binary collisions of free and bond electrons showed that the preformed plasma has a significant impact on generation of electrons and their transport. In particular, a longer scale length preplasma significantly reduces the energy coupling from the intense laser to the wire due to the larger offset distance between the relativistic critical density surface and the cone tip as well as a wider divergence of source electrons. We also observed that laser-driven plasma ionization increase in the LPI region can potentially alter the electron density profile during the laser interaction, forcing the electron source to be moved farther away from the cone tip which contributes to the reduction of energy coupling. In addition, The effect of using cones in an environment with heavy blow-off plasma outside the cone by using cones with varying wall thickness, in particular, comparing "thin" (12 μm cone wall) and "thick" cones (160 μm) was also investigated using the Titan laser. We found that thick cone walls reduced the energy coupling by a factor of up to 4, and an increase of pre-pulse inside the cone by a factor of 50 further reduced the coupling by a factor of 3[**Akli12b**]. We performed numerical simulations free of adjustable parameters by using FLASH [Fryxell00] to model the preplasma density, temperature and ionization state profiles inside the cone and LSP/ITS to model the LPI and subsequent electron propagation. The same trends were observed with reasonable agreement between the measured and modeled Kα profiles along the wire. Due to the presence of preplasma inside the cone, it was found that the trajectories followed by the electrons were significantly different for the two cases. Thick cones provided greater opportunity for electrons to become "lost" and never couple into the wire. This further highlights the detrimental effects of laser prepulse on the forward energy coupling.

Campaigns at the Trident lasers [**Higginson10**, **12**, **13**] in which the pre-pulse level was reduced to E_{pre}~ 1μJ, showed the energy coupled from a gold cone into a Cu wire at its tip increases by 2.7× over the case for E_{pre} ~10mJ, and and decreases ~8× for E_{pre}~1J (Fig. 15). To quantitatively compare with the experimentally measured Kα emission profiles, the ectrons from the LPI simulations using the LSP code crossing the inner-cone tip are recorded in time, space and momentum. These electrons are then passed to the inner cone-tip of full-scale transport simulations also done using LSP, now in a 2D cylindrical geometry to correctly model the evolution of fields along the wire boundary, which would not be correct in 2D Cartesian geometry. The electrons undergo collisions treated through a test particle model[Atzeni09] with the addition of radiative stopping[Groom00] and Kα generation cross sections[Hombourger98]. The background Au/Cu ions and electrons are modeled as fluid particles with an equation-of-state (EOS) from PROPACEOS [MacFarlane06] and temperature-dependent collision frequencies [Lee84, Desjarlais01]. The cone extends backwards 300 μm from the tip and the 1.5 mm wire is completely included, both are modeled at solid density. Vacuum boundaries of 1 mm are extended from the edges of the target to ensure that the electric field development is completely modeled. The results of these simulations are shown in Fig. 16 compared to lineouts taken from the Kα imager. Here the energy of the injected electrons has been varied to match the peak Kα yield and the lineouts have been convolved with the response function of the imager. Notice that the initial falloff of the Kα emission varies noticeably with the different initial preplasma profiles. The electron spectrum from the 3 μm case is the best fit to the Trident data from which we can infer that 23% of the laser energy is coupled into electrons reaching the inner cone-tip of all energies, while 5.5% is coupled into electrons in the 1-3 MeV range of particular interest to FI. We find that the coupling of electron energy is increased substantially using the high-contrast laser, as compared to low-contrast cases, in a FI cone-geometry. The reasons for this are the decreased distance from the inner cone-tip and a suppression of non-linear effects in the preplasma. It should be noted that compared to previous work [**Ma12**], these new simulations matching experimentally measured Kα yield and spatial profile along the wire have used a more complete physical model, including proton contaminants on the wire, electron angular divergence and a LPI-simulated electron energy spectrum. *Altogether, and including the enhancement gained from high-contrast laser pulses, our results of high energy coupling through the cone tip show a much brighter picture for FI feasibility.* A manuscript [**Higginson13**] is currently under review with the journal Phys. Rev. Lett.

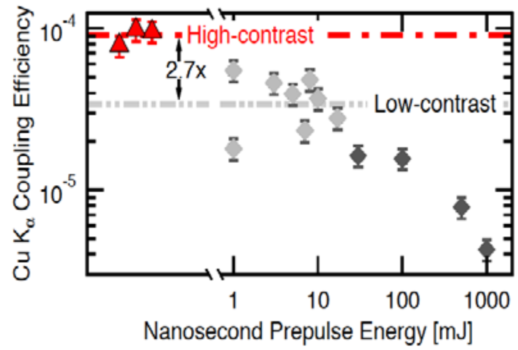

Fig. 15: Experimental laser-to-K x-ray coupling efficiency from the high-contrast Trident laser (triangles) [**Higginson13**] and the low-contrast Titan laser (diamonds). Light shaded diamonds were taken with the intrinsic prepulse of the laser (1 - 17 mJ), while darker diamonds[**Ma12**] were taken with injected prepulse (up to 1 J). The double and triple dot-dashed lines are averages of the intrinsic prepulse cases.

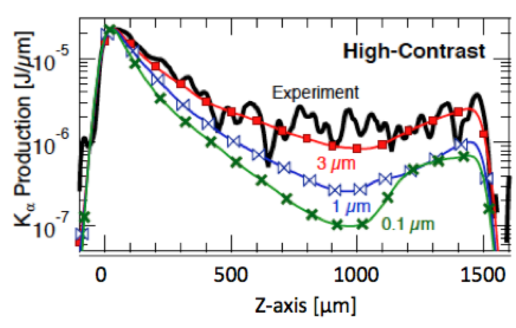

Fig. 16: Cu Kα x-ray emission lineouts from the Cu wires. Lineouts from 5×10^{19}W/cm^2 with Trident experimental data as a solid line and simulated data of the 0.1, 1 and 3 **μ**m scale length preplasma cases.

3.2. Fast electron generation and transport in FI relevant conditions

Relativistic ignition electrons, in FI scheme, have to propagate in plasmas over a gradient in density from critical (~10^{21}cm^{-3}) to ~10^{26}cm^{-3} and temperature from a few eV to 5keV over 10's–100's µm distance. Both kinetic and collisional/resistive effects can occur and modify fast electron transport, which is dependent on both the temperature and density of transport materials. In the last 3 years, we have carried out experiments with solid targets to investigate material and laser pulse length effects using the 10 ps kilojoule OMEGA EP laser. Significant progress has been made in creating and characterizing warm dense plasma platform driven by the high energy laser driven shock heating of low density foam targets. Study of fast electron transport in such plasma media has been carried out on both the Titan laser and the OMEGA EP laser. A novel Cu-doped CD shell was created for an OMEGA campaign [**Key08**] to allow direct comparison of electron coupling with neutron-measured core heating in an FI cone-shell target.

3.2.1. Dynamics of fast electron generation and transport on laser pulse length

The object is to study the dynamics of fast electron generation and transport dependence on laser pulse length extending the parameters space from sub-ps to FI relevant 10 ps.

Until recently, most studies were conducted with sub-ps laser pulses with energies of ~0.1 kJ. Through a series of experiments on OMEGA EP laser at LLE with a wide range of parameters (τ_L~ 0.7 – 10 ps, E_L~0.1 – 1.5 kJ, I_L up to 4×10^{19} W/cm^2, and with intrinsic nanosecond-scale prepulse energies of 0.1 – 100 mJ), we have extended the study of fast electron generation and transport from sub-ps to FI relevant 10 ps pulse duration at higher energy level. The multilayered solid targets had an Al layer (~ 100 µm) and a Cu tracer layer (~ 20 µm) backed with a 1mm thick 5×5mm^2 wide conductive carbon layer to minimize electron refluxing. Fast electrons were characterized through recording of Cu Kα with a monochromatic 8keV x-ray imager, an x-ray spectrometer for absolute Kα yield.

The first set of shots with the low contrast pulse (prepulse energy of up to ~100 mJ) clearly showed that *with increasing pulse length (0.7, 3, and 10 ps), the laser-generated electron beam breaks up into an increasing number of filaments* (Fig. 17) *of decreasing size*. The single beam from a sub-ps LPI has a full width half maximum (FWHM) spot size of ~160 µm, while narrow beamlets have an average size of ~70

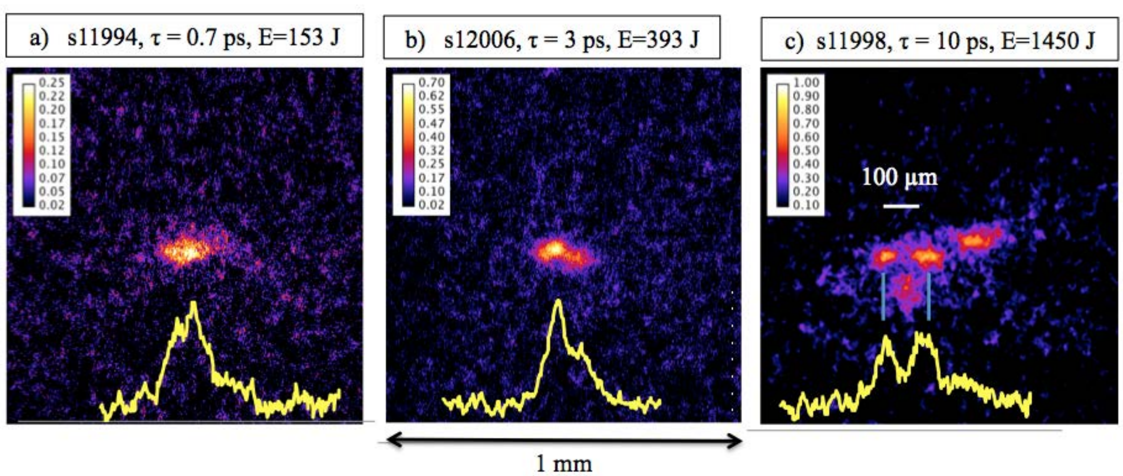

Fig. 17: Cu K_α images showing fast-electron beam cross-section ~100 µm below the generating point using a laser pulse of (a) 0.7 ps, 153 J, (b) 3 ps 393 J, (c) 10 ps 1450 J pulses in the OMEGA EP experiment. All images are to the same spatial scale. Image is compressed vertically because of the view angle. The yellow lines at the bottom of each image are plots of the pixel intensity along a horizontal line through the points.

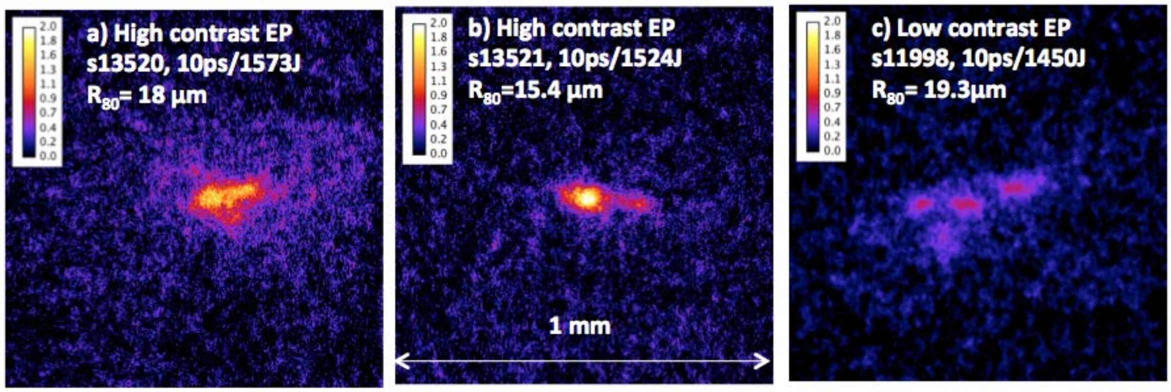

Fig. 18. 2D Kα images observed in 10 ps LPI with identical targets (a) and (b) using the high contrast EP pulse (ns prepulse energy ~ 1 mJ), and (c) with the low contrast (prepulse energy ~ 110 mJ) EP laser beam. Images are on the same spatial and color scale. More fined electron beam with brighter peak signal were observed compared to the filamented beam in the low contrast case.

µm (FWHM), which might indicate that the filamented beam could be further collimated by the self-generated resistive B-fields growing with time inside the solid density target. Kα images from the LPI with 3 ps pulses started to show secondary features near the main beam. The very large angular separation (>40°) between these relatively narrow filaments shown in Fig. 17(c) for the Kα image observed in a 10 ps shot is quite surprising.

It should be noted that the energy in the 3 ns long pedestal prepulse was also varied, i.e., 5 mJ, 16 mJ and 110 mJ for the increasing energy of the low contrast EP pulse with durations of 0.7ps, 3 ps and 10 ps, respectively. It is expected that there was a significant amount of preplasma as the result of 110 mJ, 3 ns prepulse in the 10 ps interaction case. Strong nonlinear laser plasma interaction processes such as filamentation, hole-boring and hosing instabilities may occur in the extended preformed plasmas over 10 ps pulse duration which could lead to the formation of the widely separated electron filaments observed in the experiments as discussed below.

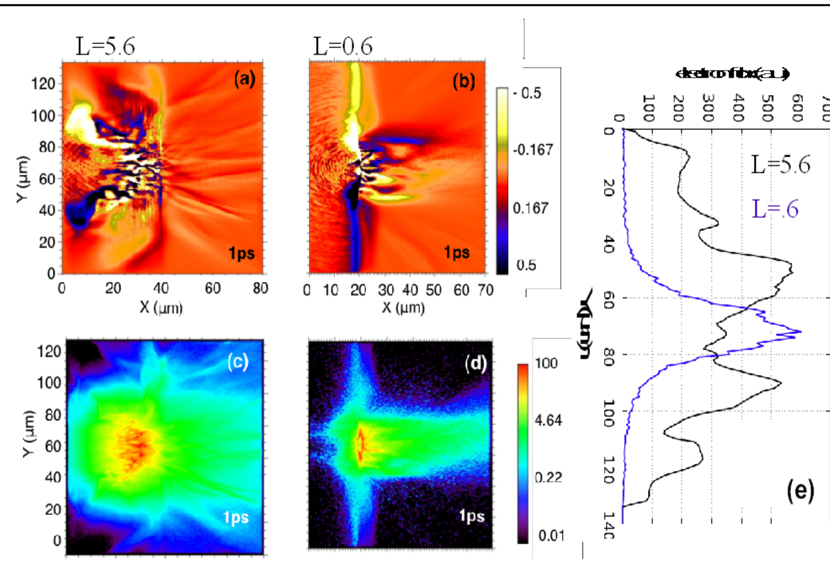

Fig. 19: PICLS azimuthal B-field comparison in low and high contrast laser cases for L = 5.6µm (a) and L=0.3µm (b) at 1 ps, respectively. A confined electron beam guided by self-generated reisistive B-field is observed with insignificant pre-plasma. Electron energy density for L = 5.6 µm (c) and L=0.6 µm (d) targets at 1ps. (e) fast electron beam profile at 35µm inside solid front surface averaged over whole laser pulse duration (2 ps).

2D Kα images from the 2nd set of experiments in FY13 with the *high contrast* (prepulse energy < 1 mJ) *EP beam* as shown in Fig. have verified that the multiple angularly separated electron filaments were indeed caused by instabilities during LPI over

10 ps duration with the presence of a large preplasma. As shown in Fig. 11, Kα image data clearly showed that ***a more confined electron beam was produced from the clean interaction with a steep density gradient in the10 ps LPI case with the high contrast EP pulse***. Also noted is the higher signal level in the Kα intensity in the confined electron beam compared to that in the spread-out filamented beam in the LPI with the low contrast case (Fig. 18c). PICLS and LSP simulations are underway to examine the LPI and fast electron generation and transport. *These new findings emphasize the requirement of the high contrast capability of the high-energy high-intensity laser pulse to avoid the unnecessary LPI instability for more confined electron beam generation leading to higher delivered intensities.*

PICLS simulations have been performed to examine laser plasma interaction and fast electron generation over 2 ps and compares electron beam behavior in the interaction of a high-contrast laser (almost no pre-plasma; L=0.3μm) versus a lower contrast beam containing significant pre-pulse (L=5.6μm, comparable to the experimental preplasma condition) with planar-Al target. Modeling shows that in clean interaction (no pre-plasma) the electron beam divergence is small resulting into higher on axis current density and resistive B-fields produced from such current are strong enough to confine and collimate the beam as time passes, see Fig. 19 (b) and (d). However, laser interacting with large pre-plasma becomes filamented and these filaments deviate from their original direction and sprays electrons in wide area as clearly seen in Fig. 19 (a) and (c). Moreover, with large pre-plasma absorption occurs much farther from the solid surface resulting in to widely diverged electron beam with lower current density. Inside the solid density target due to resistive filamentation instability the beam further breaks up into widely separated self-pinched multiple channels. Fig 19(e) compares the electron flux transverse profile, collected in 1μm wide box located 35μm inside from solid surface, for all electrons with energy above 100 keV, which clearly show multiple beamlets feature in the long scale-length preplasma for the low-contrast case and a more confined electron beam with the high contrast (almost no pre-plasma) case. These observations are consistent with the experiments and are being summarized for publication.

3.2.2. Dependence of fast electron transport on target material and magnetic collimation

The object is to study transport dependence on target material and fast electron collimation by self-generated magnetic fields.

With the high contrast EP pulse, we have also extended our previous work on resistive collimation with laser pulses at sub-ps on both Titan laser (150J, 0.7 ps) [**Chawla13]** and Omega EP (300 J, 1 ps) [**Wei12**] to 10 ps pulse duration at kilojoule energies [**Wei13a, b**] using a high-Z transport target which has a thin (a few μm) Au layer embedded about 10 μm beneath the Al substrate. 2D collisional particle-in-cell simulations using the PICLS code showed formation of strong self-generated resistive magnetic fields in

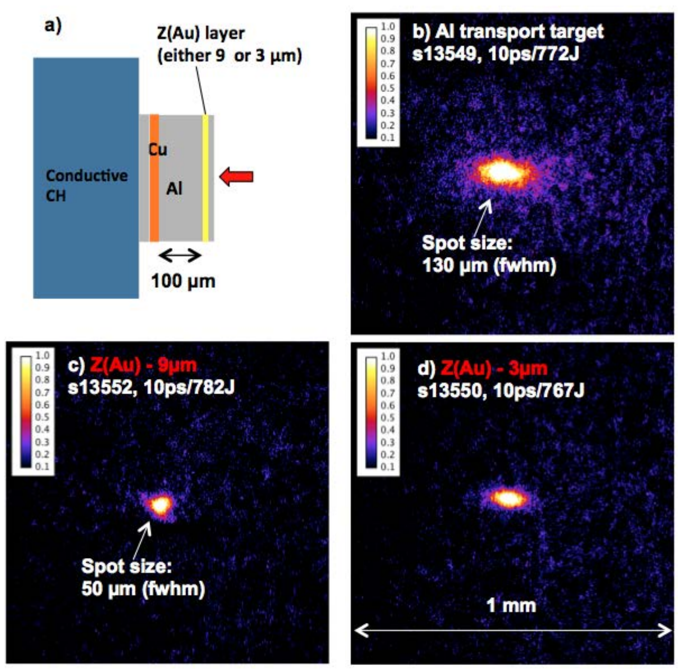

Fig. 20. a) multilayered planar foil target with Z(Au) transport layer and the measured Kα images from the 10 ps interactions using the high contrast EP pulse a) from the Al transport target without high-Z Au layer and c), d) from the Z(Au) transport targets with 9 μm and 3 μm Au layer respectively.

targets with a high-Z transport layer that suppressed the fast-electron beam divergence; the consequent magnetic channels guided the fast electron transport [**Chawla13, Mishra13**]. 2D Kα images as shown in Fig. 20 c) and d) from such targets illuminated by the 10 ps high contrast EP laser tightly focused at the flat target surface have clearly shown a better collimated electron beam compared to that with the Al transport target case (Fig. 20b). *A remarkably stable and collimated electron beam with spot size as small as 50 µm after >100 µm propagation distance with a full angular divergence of 20° has been demonstrated for the first time for fast ignition relevant 10 ps pulses.* Such magnetic fields may be produced by adding structures in the cone tip to collimate electrons in cone-guided FI relevant condition [Robinson07]. Several manuscripts are currently being prepared for publications in high quality journals.

3.2.3. Study of fast electron transport in heated plasma

The objective is to investigate transport properties of fast electrons penetrating into warm dense plasmas.

Electron transport study from shocked gold into warm dense plasmas at 1g/cc using the Titan laser and 30mg/cc using the OMEGA EP give indications of wide electron spreading on transition from dense gold into heated foam plasma. This experiment has been benchmarked with PIC code PICLS [**Wei**10, **Wei**13c]. Experiments on OMEGA EP showed significant stopping in low-density (30mg/cc) background plasma [**Yabuuchi11**, **13b**, **Beg12a**, **12b**].

<u>Transport into 1g/cc</u>: The Titan LP beam (E~300J, τ~3ns square pulse) drove a shock from the backside to compress a CRF foam ~8× to thickness δ~15µm (diagnosed using side-on point projection radiography [**LePape**08] (Fig. 3.2-1b)). When the shock arrived at the front Au layer (δ~5µm) Titan SP (E~150J, τ~0.7ps, I_{peak}~10^{20} W/cm^2) was fired to create electrons in the Au layer (δ~5µm) (Fig. 21a). Electron-induced fluorescence from a Cu tracer layer backing the compressed foam diagnosed the hot electron flux. Comparisons were made uncompressed foam and full density, cold CH replacing the foam.

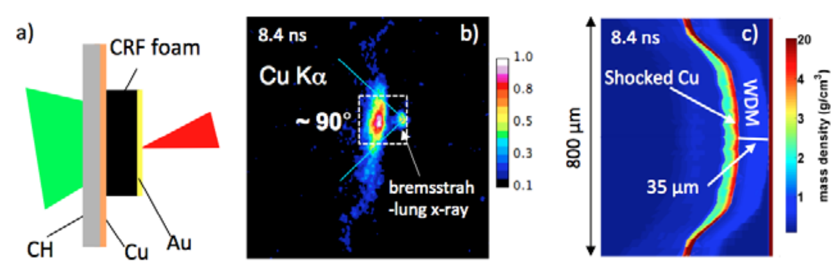

Fig. 21: Large angular spread of electrons observed in transport through WDM. a) schematic of lasers (long pulse in Green and short pulse in Red) and foam package target; b) Side-on 8keV x-ray emission data showing a lateral FWHM Cu-$K\alpha$ fluorescence spread of ~ 188µm. The marked square box is 200µmx200µm; c) h2d simulated mass density plot of the shocked Cu and WDM at the same

A large $K\alpha$ spot was consistently observed in all the shots when the fast electrons travelled through warm dense matter (Fig. 21c), but not in the cold targets. In the warm target the width w~158±20 µm FWHM transverse size (correcting for self-absorption) is ~2× larger than that measured with initially cold (Al, CH) targets with the same laser condition. At the peak bremsstrahlung emission spot location the fast electron emission divergence angle is θ_{half}~46°. This is significantly larger than that inferred previously in the cold solid target experiments [Stephens04, Lancaster07], but consistent with the large beam divergence predicted by PIC simulations [Kemp10, Debayle10].

PICLS simulations using experimental laser and plasma conditions show that the electrons are produced with a wide angular spread in laser absorption region as seen in electron energy density plot at 1ps in Fig. 22(f). In early stages of laser interaction with the front low density plasma, high energy electron escaping from laser focal region in transverse direction set up an electrostatic field (similar to a sheath field) enveloping laser focal region due to the charge imbalance. Fig. 22(a) and (b) show the quasi-static azimuthal B-field and transverse electrostatic field (E_y) snap shots at 160τ_L, here the peak value of E_y is as large as ~ 8x10^{-11} V/m. This growing E-field is accompanied by strong magnetic field according to $dB/dt = \nabla \times E$. Strong azimuthal B-fields (~ 100-200 MG) are produced at the front surface. Fast electrons escaping laterally from the focal region were likely to be deflected by B-field and start orbiting to form current loop in sideways which is inferred from PICLS produced current density profiles. The transverse current densities J_y and J_x are plotted in Fig. 22 (c) and (d), respectively, here black/white dashed arrows indicates electron flow direction in LPI region. In warm dense (WD) region (representing coronal plasma in FI scenario) resistive electromagnetic fields (peak B-field ~ 1-5 MG) are not strong enough to affect the relativistic electron dynamics significantly, see B-field snapshot at 1 ps in Fig. 22(e). The shock compressed WD region has an ion, i.e. carbon (Z=6), density n_i ~ 50n_c suggesting that in such moderately dense background the kinetic effects will also be damped. Therefore, we also do not observe any kinetic effects, such as electromagnetic waves resulting from various kinetic instabilities. It is observed that source electrons propagate almost ballistically and likely to maintain their source divergence, see Fig. 22(f). The fast electron divergence at the observation point is determined by the source divergence (> 45° half cone angle) and consistent with what is inferred in the experimental. An article [**Wei13c**] summarizing above work is under review for potential publication in Physics Review Letters.

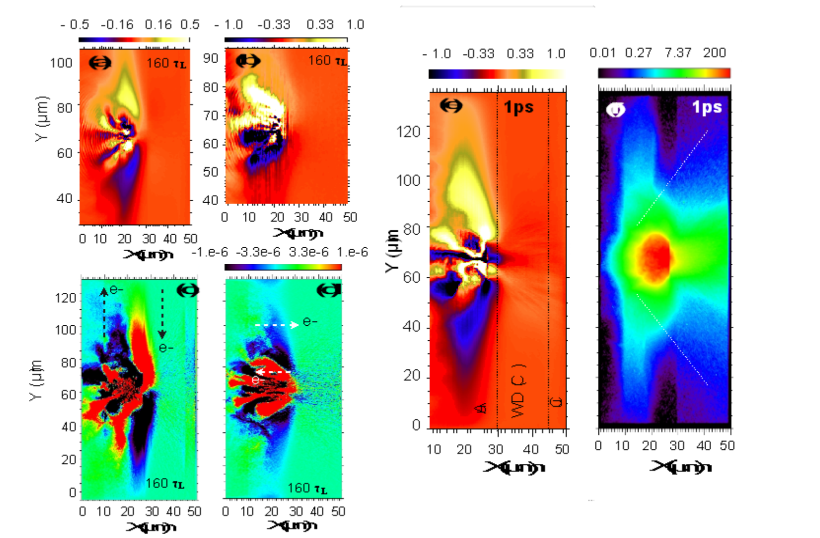

Fig. 22: PICLS results for quasi-static (a) azimuthal B-field (Bz) (b) transverse electrostatic field (Ey) in the units of 107 MG and 3e12 V/m respectively plotted at 160τ_L. Strong sheath like field is produced enveloping self focused laser light in lower density plasma. (b) and (c) are longitudinal (Jx) and transverse (Jy) current and black/white dotted arrow represent electron flow direction. 1 ps results for (a) azimuthal B-field (Bz) and (b) electron energy density showing not significant field and ballistic motion of electrons in WD region.

Transport into 30 mg/cc: The electron angular spread and energy transport was examined at OMEGA EP in a large (~250×400×250μm^3), hot (~40 eV) and low density (30 mg/cc

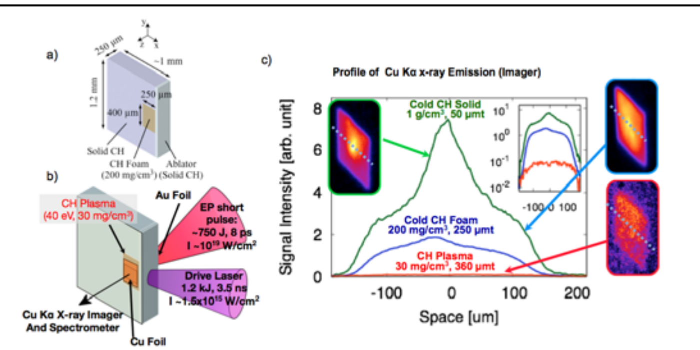

Fig. 23: (a) Schematic of the foam package target. Plastic-coated gold foils on both sides were added for fast electron transport in laser driven foam experiment b). The holes were covered with gold and copper foils in the transport experiment. Fluorescence from the Cu foils (c) was much weaker for the hot plasma than for the two cold reference shots.

correspond to $7n_c$) plasma [**Yabuuchi11, 13b**]; CH foam with original density of 250 mg/cc in a plastic container (Fig. 23a) which was shock compressed in one dimension, then re-expanded to create the approximately uniform profile. PRISM Spect3D [Prism] analysis of absorption spectroscopy verified the 2-D DRACO rad-hydro code predictions, though the density (30mg/cc) was lower than expected [**Sawada**12, **Yabuuchi12**].

Fluorescence images from electrons traveling through this plasma (Fig. 23b) and two other reference configurations showed a well defined beam, giving a small spot for 50 μm thick CH and a proportionally larger spot for 250 μm thick CH foam (with same areal mass), but no clear structure, and much lower (25X weaker) intensity (Fig. 23c) when plasma was the transport medium. The large divergence is consistent with the observation described in previous section. Particle-in-cell simulations using the OSIRIS code [Fonseca02] in collaboration with Prof. W. Mori's group at UCLA were conducted to model fast electron transport in the heated foam case included source generation, transition into the plasma, transport within the heated plasma, and refluxing. Simulations identified several mechanisms that limit the number of fast electrons that can traverse the plasma. The dominant mechanism is longitudinal inhibition due to strong electric fields at the solid Au and low-density ($7\ n_c$) plasma interface. Transverse spreading caused by $E \times B$ drift at the interface is also significant, which agrees with the experimental observations. An article [**Yabuuchi13b**] summarizing above work is under review for potential publication in Physics Review Letters.

The hot electron transport results in warm dense matter clearly indicate that the hot electron dynamics in warm dense plasmas is significantly different than in cold, solid targets. This study is extremely important for the FI cone tip/compressed fuel interface and warranted a detailed investigation in integrated experiments with information about the spatial distribution of hot electrons coming out of cone tip discussed in next section.

3.2.4. Integrated study of electron spatial energy transport in imploded high density plasmas

The objective is to use the fluorescence from a Cu doped shell to directly characterize electron propagation into the imploded hot dense plasma using a cone-in-shell target.

We have developed a platform on the Omega laser facility to better characterize fast electron spatial energy coupling into imploded high density plasmas by adding Cu dopant to the inner part of the CD shell and observing fast electron induced Cu fluorescence emission from the imploded high-density plasma. The 2D imaging system records the 8 keV Cu Kα emission image [Stoeckl12a, Stoeckl12b], and an absolutely calibrated Zinc Von Hamos (ZVH) x-ray spectrometer tuned for Cu K-shell and ionic line emission measures the total Cu Kα yield. Using this new platform, we have investigated two main issues with fast electron transport into imploded FI cone-in-shell targets. The first is the spatial distribution of the fast electrons as they propagate into the compressed core and the second is the energy coupling of those fast electrons to the compressed core.

The cone-in-shell targets consist of a Cu-doped CD shell with outer diameter of 870-μm attached to a gold cone (34° angle, 10-μm tip diameter and 15-μm tip thickness). The target parameters (shell and cone) are identical with the targets that have been used and gave the best performance on the neutron yield in the OMEGA integrated FI experiments [**Theobald11**]. The CH/CD shell consists of a 15-μm thick outer CH ablator layer and a 23-μm thick inner CD layer that is doped with Cu (at ~1% atomic density). The CH ablator thickness was chosen to reduce direct interaction of the driver beam with the Cu-doped inner layer to minimize the Cu He-α line emission and facilitate the Cu Kα spectrum measurement by the ZVH spectrometer. Implosion of cone-in-shell target was achieved using 54 beams of the OMEGA laser (18 kJ, 2.7 ns) with a low adiabat pulse shape while the high intensity short pulse OMEGA EP laser (up to 1.4 kJ in 10 ps) was focused inside the guiding cone to produce fast electrons with various injection times, i.e., 3.65 ns to 3.85 ns relative to the OMEGA driver beam. To verify target performance, 2-D radiation hydrodynamics simulations using the DRACO code were performed to model the implosion and fuel assembly of this specialized target and provide the guidance for the short pulse injection time in the experiment. It was confirmed that the shock breakout time at the inner cone tip and the achieved density at peak compression time were similar to the targets used by Theobald et al, for which the shock breakout was measured to occur 3.76±0.03 ns after the implosion laser was incident. According to the simulations the maximum areal density was about 0.3 g/cm^2 in the axial direction opposite to the cone. The peak density at the maximum compression was ~100 g/cm^3.

We obtained for the first time clear images of fast electrons' spatial energy deposition in the imploded plasmas [**Jarrott12, Jarrott13, Beg13**]. The induced Cu Kα emission attributable to OMEGA EP produced fast electrons was found by subtracting the emission image of an OMEGA-only shot from each of the joint shot images. Fig. 24 exhibits these images, zoomed in around the imploded shell center region from three joint shots with the OMEGA EP beam at ~ 500 J energy injected at three different time delays (i.e., 3.65 ns, 3.75 ns and 3.85 ns) relative to the OMEGA driver which spanned the time at which time the inner cone tip was broken by an implosion-driven shock as predicted by the 2D DRACO simulations [Radha05, Solodov09] and validated using the SOP/VISAR diagnostics in the previous experiments [**Theobald11**]. These 2D Kα images clearly show that fast electrons penetrated through the cone (wall and tip) into the compressed shell producing strong Cu Kα emission from the region of the imploded high-density plasmas. The observed decreasing fluorescence emission size in the SCI images with the increasing OMEGA EP time delay is consistent with the simulated density profiles of the imploded shell at the corresponding implosion time in the 2D radiation hydrodynamic modeling results (also shown in Fig. 24) using the DRACO code. It should be pointed out that the peak emission from the dense shell outside the side cone wall is not at the cone tip, but ~ 100 µm up the cone walls which is consistent with HYDRA modeling predicted level of preplasma filling of the cone as a result of the intrinsic 3-ns long prepulse with an energy of ~ 20 mJ prior the main pulse. It was also observed that the Cu Kα emission was reduced in the region of the core in front of the cone tip. The possible causes could be the reduced collection efficiency of the SCI due to the shifting and broadening of the Cu Kα spectral line at plasma temperatures above the order of 150 eV and/or the deflection of fast electrons by self-generated B-fields.

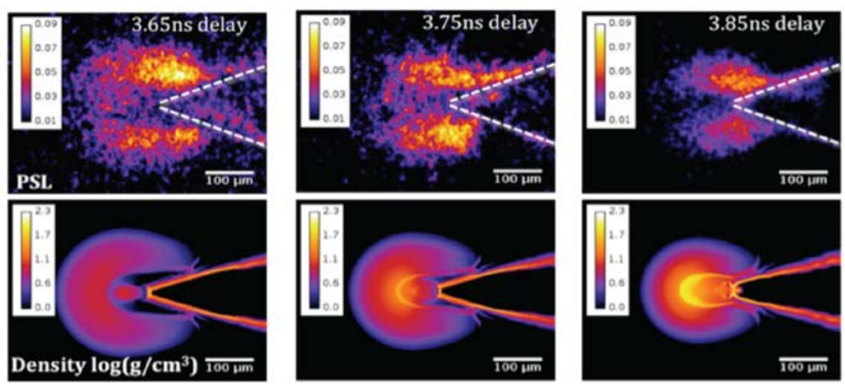

Fig. 24: (top) Cu Kα images showing the emission from the vicinity of the cone tip at various delays with the OMEGA EP beam energy at ~ 500 J. The dotted triangles are added to visualize the cone position and the dotted bar shows the estimated emission spot radius; (bottom) plots are the calculated mass density (in units of log g/cm^3) maps from DRACO simulations. Also note the significant reduction in Cu Kα yield at 3.85 ns for the OMEGA EP delay corresponding to after the cone-tip breakout by the implosion.

Calibrated x-ray spectrometer data provided measurements of spatially integrated Cu Kα yield (due to both OMEGA EP produced MeV fast electrons and the OMEGA driver produced suprathermal electrons with energy of 20-30 keV) which is less sensitive to plasma temperature. Fig. 25 shows fast electron induced Kα yield enhancement as a function of EP beam energy (Fig. 25a) at a fixed timing delay at 3.65 ns and the timing delay scan at a fixed EP beam energy of 500 J (Fig. 25b) with the high and low contrast pulses. The total Cu Kα yield *increased significantly (up to 70%)* in the joint shots compared to the OMEGA only implosion shots as the result of fast electrons propagating into the high density plasma. Except for one data point in which the signal and background were anomalously low (1 kJ high contrast point, currently under investigation), fast electron energy coupling to the compressed core was found to *increase with the OMEGA EP beam energy* and coupling was *increased with high contrast* particularly at high laser intensity with > 1 kJ energy. In Fig. 25(b), note the increase in yield with delay time until the latest delay, 3.85 ns indicating the EP injection time can be tuned to control fast electron coupling. The decrease at 3.85 ns is due to the plasma filling of the cone after the implosion driven shock breaks the cone tip consistent with DRACO simulation prediction and SOP/VISAR measurement from previous experiments [**Theobald11**].

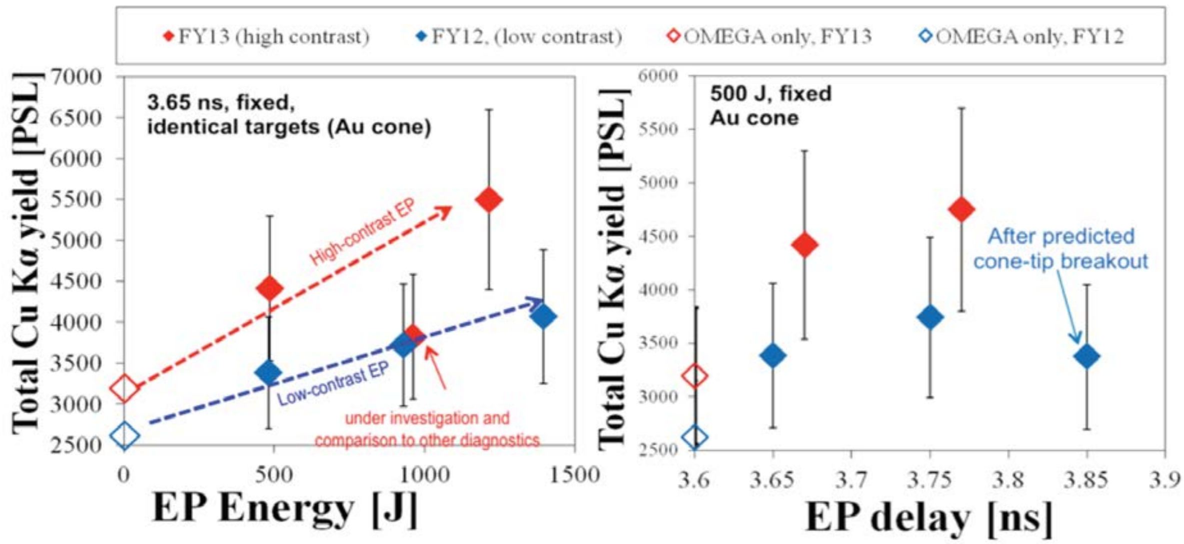

Fig. 25: Comparison of Cu Kα yield enhancement due to fast electrons measured by the ZVH x-ray spectrometer as a function of EP beam energy at a fixed delay of 3.65 ns (a) and as a function of EP timing delay at a fixed EP beam energy (500 J) (b) in similar experiments with the identical OMEGA driver and standard Au cone-in-shell targets with Cu dopant using the high contrast (ns prepusle energy < 1 mJ) and the low contrast (prepulse energy ~ 100 mJ) EP pulses.

These new results are the *first direct measurements* showing the spatial energy deposition of fast electrons into an imploded high-density plasma core in the cone-guided FI configuration. Detailed analysis combining these measuremnts and LSP modeling [**Qiao13**] of LPI with realistic experimental preplasma and EP laser parameters for fast electron generation and transport modeling using both the LSP and ZUMA codes are underway to facilitate the transport physics understanding and recover the full spatial distribution and energy coupling of fast electrons into the core.

3.3. Integrated Target Core-heating Experiments

3.3.1. Integrated cone-in-shell tests of core heating efficiency

Integrated fast-ignition core-heating experiments on OMEGA (E~1kJ, τ~10ps) showed that ~3.5% of the short-pulse laser energy is coupled into the compressed plasma [**Theobald**11]. Figure 26 shows enhancement of the neutron yield by more than 4× (1.4±0.6×10^7 additional neutrons) for properly timed pulses on the smaller-tip targets. Neutron enhancement for larger tip targets is uncertain due to limited number of shots. Shock-breakout measurements performed with the same targets and drive conditions demonstrated an intact cone tip at the time when the additional neutrons were produced. DRACO simulations (of fuel assembly) [Radha05, Solodov09] + LSP simulations (of fast electron propagation and energy deposition) yielded insight into the coupling mechanism of the fast electrons to the compressed CD [**Solodov**09, **Theobald**11]. Similar to the experimental observation, the injection time of the fast electrons was chosen -50 ps before shock breakout at a time when the shock wave was transiting through the cone wall. A simple exponential energy distribution was assumed for the fast electrons with a mean energy given by the maximum of the ponderomotive [Wilks92] scaling. The total energy of the fast electrons generated at the inside cone wall contained 16% of the OMEGA EP beam energy with a fast-electron temperature of ~0.3 MeV. Due to relatively low slope temperature of the assumed electron spectrum, fast electrons were found to deposit more than 50% of their energy in the cone tip and wall, and most of those transmitted deposited their energy in the lower-density plasma (>2g/cm^3) close to the tip of the cone. The simulation obtained a neutron-yield enhancement of 1.4×10^7, which required that 3.5±1.0% of the OMEGA EP energy was coupled into the CD by fast electrons. Some fraction of fast electrons left the target without significant heating. According to the simulation, only about 0.4% of the OMEGA EP energy coupled to densities above 100 g/cm^3. It should be noted that these simulations were done without radiation cooling and used a simplified electron energy spectrum.

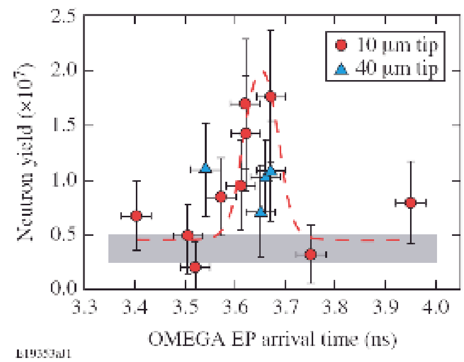

Fig. 26: Measured neutron yield as a function of the arrival time of the short-pulse laser for 10µm (circles) and 40µm (triangles) tip diameter cone targets. The gray area represents data without the short-pulse laser.

3.3.2. Design and simulations of low-Z cone tip targets

To improve the energy coupling, a new aluminum cone tip target has been designed and modeled with detailed simulations using the DRACO code with improved physics models of laser beam energy absorption (e.g. cross-beam energy absorption) and radiation transport. Fig. 27 shows a DRACO simulation of a cone-in-shell target with an aluminum block mounted in front of a gold cone. A very thin (~2 µm) gold layer inside the cone tip serves as a mounting layer for the block and also helps to shield radiation. This very thin gold layer has no significant effect on the transport of the fast electrons. The gold cone has an inner full opening angle of 34°±1°, a sidewall thickness of 15 µm, and a 40 µm small circular inner flat tip. The cylindrically shaped Al tip is 60 µm thick on axis and 80 µm in diameter. The cone tip in a previous design [**Theobald11**] was made out of 15 µm of gold. The hollow gold cone is inserted into

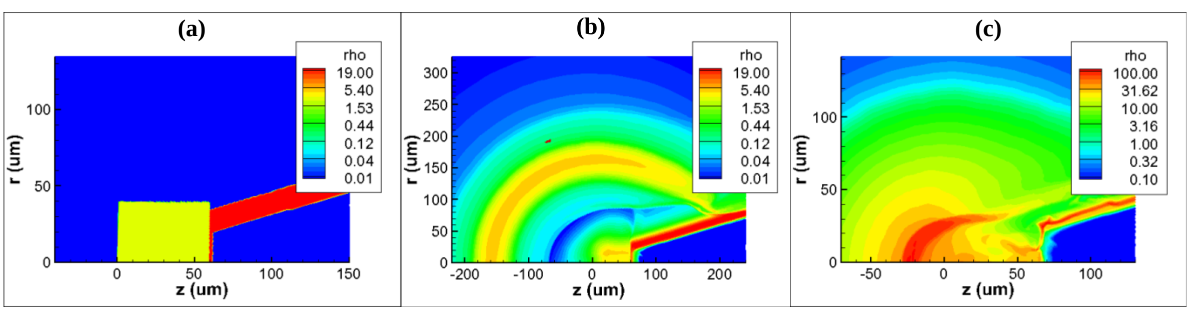

Fig. 27: 2-D hydrodynamic simulation of a cone-in-shell target with the code DRACO [Radha05, Solodov09]. (a) Detail of the tip showing the gold cone and aluminum tip. (b) Imploding shell at 3.25 ns, before peak compression. Simulations predict thermal expansion of the cone material due to radiation preheat. The aluminum tip expands faster than the gold material. (c) Density map at a later time of 3.87 ns (0.19 ns before peak compression) showing better shock resilience of this design than the previous Au cone tip target.

a 42-µm thick plastic shell (14-µm outer CH layer and 28-µm inner CD layer) with an outer diameter of ~870-µm, which is filled with 0.8 atm of air. The simulated breakout at 3.78 ns is very close to the measured breakout time (3.85 ns). The time of peak compression, however, is reached at 4.06 ns or 190 ps *after* the tip is destroyed. This design is more resilient against the strong shock from the implosion than the previous design with a gold-only cone [**Theobald11**]. Similar, improved simulations were performed for the Au cone cone-in-shell target. This also suggests that, from a hydrodynamic point of view, the neutron yield enhancement (see Fig. 26) could have been limited by an early destruction of the cone tip. In the new design, the tip is made of aluminum, and is significantly thicker than the Au tip. More mass on axis helps to delay the shock breakout closer to the time of peak compression and increases the margin for the arrival of the short-pulse laser. The hydrodynamic simulations show that the shock breaks through first on axis, which was also observed in other modeling work [Honrubia10]. Al as opposed to Au for the tip should also provide better electron transport despite being thicker. Several detailed studies with DRACO and LSP have been performed to confirm this and improve the design. For example, designs using simply an Al tip inserted into the Au-cone suffered from Al plasma filling the cone even before shock breakout. This was mitigated by mounting a thicker Al block in front of the cone leaving a thin (~2 µm) intermediate gold layer, which serves as radiation shield and effectively stops the x-ray radiation from the corona entering the cone. This prevents preplasma from forming inside the cone. Fig. 27(c) shows that the interior of the cone volume is plasma free up to the time when the shock breaks through.

3.3.3. Validation experiments of the low-Z cone tip targets on OMEGA

A backlighter platform validates the 2-D radiation–hydrodynamic modeling predictions of the compression of cone-in-shell targets using the joint OMEGA and EP facility [**Theobald12**]. The technique uses flash radiography with a monochromatic 8 keV x-ray source to measure the fuel assembly of imploded cone-in-shell targets with Al tip. 54 out of the 60 OMEGA UV laser beams with energy of ~18 kJ imploded the capsule using a low-adiabat drive pulse shape [**Theobald11**]. Simultaneously, a thin Cu foil was irradiated by the 1.5-kJ, 10-ps OMEGA EP short-pulse laser and generated a bright Cu Kα backlighter source. A spherical Bragg crystal located on the opposite side of the target imaged the cone-

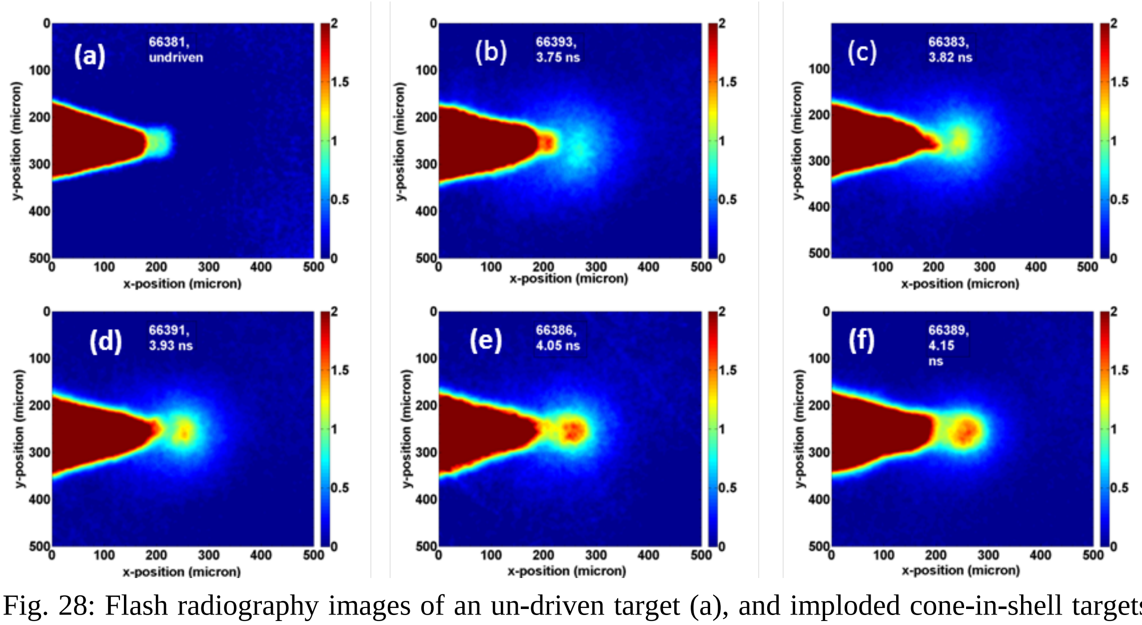

Fig. 28: Flash radiography images of an un-driven target (a), and imploded cone-in-shell targets at various stages of the implosion at 3.75 ns (b), 3.82 ns (c), 3.93 ns (d), 4.05 ns (e), and at 4.15 ns (f) after the start of the UV drive laser pulse [**Theobald12**]. The false color scheme represents the measured optical density.

in-shell implosions onto an image plate detector [Stoeckl12b]. Flash radiography combined with monochromatic imaging provides high-quality images of the fuel assembly with 12-ps time resolution and 22-μm spatial resolution. The time resolution is given by the emission time of the Kα source, which was measured to be 12 ps [Nilson10] and the spatial resolution of the imaging system was characterized in situ with an un-driven target. Interleaved with joint shots, shock breakout measurements [Stoeckl05, **Theobald11**] were performed with OMEGA only beams. The experiments demonstrate improved shock resilience and that the cone withstands the radiation load from the implosion. Figure 28 shows measured 8 keV backlighter images of the implosion at various times around peak compression over a time range of ~0.4 ns and over a region of 500 μm × 500 μm. Fig. 28(a) shows a picture of an un-driven target, where the Al tip is clearly visible and less opaque than the gold cone. The false color scheme represents the measured optical density. The frame in Fig. 28(b) shows the implosion at 3.75 ns after the start of the drive pulse shape. The fuel starts to assemble in front of the tip and the Al tip is compressed in the radial and in the longitudinal directions to a higher density. The following frames were taken at successively later times (3.82 ns (c), 3.93 ns (d), 4.05 ns (e), and 4.15 ns (f)). With later time the Al tip is more deformed and eventually completely destroyed and the fuel assembly reaches higher density. The radiographs show how the implosion destroys and pushes back the cone tip. Peak compression was reached close to the time of the frame in Fig. 28(e), while the last frame was after peak compression. The measured time of peak compression and the measured areal densities compare well to 2-D DRACO simulations. In addition, an independent measurement of the breakout time of the shock that is driven through the cone tip agrees within 50 ps to the predicted value, which is an excellent agreement. *The measured peak areal density is 300 mg/cm^2, which is among the highest areal densities that were ever measured on OMEGA.* A manuscript is being prepared for publication.

3.3.4. Channeling studies using the 4ω probe

The evacuation of cavities in plasma by a high-intensity laser beam is of practical importance to the channeling fast ignition concept. The channel in the plasma corona of an imploded ICF capsule provides a clear path through the plasma so that a second high intensity laser can reach close to the dense core of the assembled fuel in order to achieve ignition. This study reports on experiments performed with the OMEGA EP laser using one of the short pulse IR beams (1.25 kJ, 10 ps) to form a straight channel in a large blow-off plasma with an electron temperature of ~1.5 keV that was generated by two nanosecond kJ UV laser beams. This work was done by Steve Ivancic as part of his PhD thesis work [**Ivancic11, Ivancic12, Ivancic13**]. A novel optical diagnostic employing a 10-ps, 263-nm probe laser [Froula12] measured simultaneously the background plasma density and imaged the channel. The plasma density scale length was inferred from the refraction of the probe beam showing an exponential density profile with a scale length of 275 μm **[Ivancic12**]. Figure 29 shows the measured

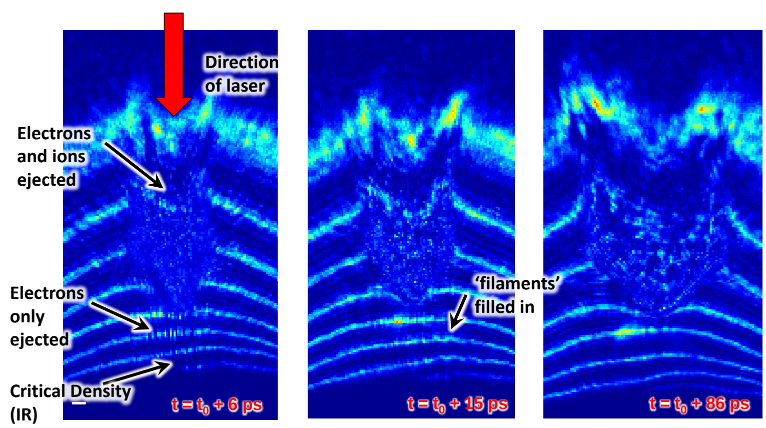

Fig. 29: Schlieren images of the channel formation for three different times of the optical probe laser (6 ps, 15 ps, and 86 ps). The picture for 6 ps was taken during the interaction of the 10 ps high intensity channeling beam. A filamentation is observed at around the critical density indicating that either fast electron currents or the optical light are transported in filaments.

schlieren images of the formed channel for three different delay times of the optical probe laser. The channel was measured to reach up to half the IR critical density with a channel width of ~ 200 μm. Images were taken at different times showing the radial evolution of a strong blast wave from the channel walls. Individual filaments were observed at the critical surfaces that indicate that the laser became unstable and broke up into multiple filaments. The rapid infilling of the 'filaments' is due to the space charge of ejecting electrons but not ions. The large cavity that persists over 100's of picoseconds is due to the ejection of electrons and ions in the low density coronal plasma. A manuscript is being prepared for publication.

3.4. Predictive Modeling Capability Development

The modeling of intense laser produced plasmas is challenging because the plasmas have extremely high densities. Because of that we need to simulate two different regimes, kinetic and collisional regimes simultaneously and self-consistently. Moreover since resistive magnetic fields are critical to determine the electron transport, the code requires the correct resistivity, which dynamically changes with ionization in plasma heating. The FI-HEDS project at LLNL has the primary role in developing integrated modeling capability – also specifically oriented to modeling the signal detected by diagnostics. Our group has been using two methods to validate the experimental data: i) The LSP code is self-consistently used to produce a hot electron source from short pulse laser matter interactions and to model subsequent transport into solid targets and ii) The PICLS code is used to produce a hot electron source from realistic laser parameters. We have done extensive modeling using the PICLS code by adding atomic physics such as impact ionization (NLTE model) and x-ray radiation. In order to carry out modeling closer to experimental conditions, preplasma density profiles for various materials were produced using the radiation hydrodynamics code HYDRA, while the cone-in-shell implosion was comprehensively modeled using the 2D DRACO code. These codes have been improved with added physics models and continuously being benchmarked against the experiments, becoming a powerful tool not only for modeling FI physics, but also beneficial to the wide HED community.

3.5. Cryogenic Target Development

The fast-ignition cryo-test stand was used to test designs and develop procedures for ice layering in targets that have a re-entrant cone. It achieves the 18K needed to solidify deuterium and has demonstrated on targets built to design specifications thermal uniformity suitable for forming a symmetrical ice layer (w/o cones) and control of the ice layer thickness. Ice layers were characterized with x-ray phase contrast images. They showed that the ice is agglomerating at the cone tip when the tip is not heated by an auxiliary source. We have demonstrated that IR layering laser power adjustment can remove the ice from the cone and obtain a layer inside the plastic shell (see Fig. 30). Further improvements in layer quality can only be obtained by filling the target with DT. It was planned on producing layered cryogenic FI cone-in-shell targets with DT at LLE. Due to limited funds and resources no further work was done on this part of the project.

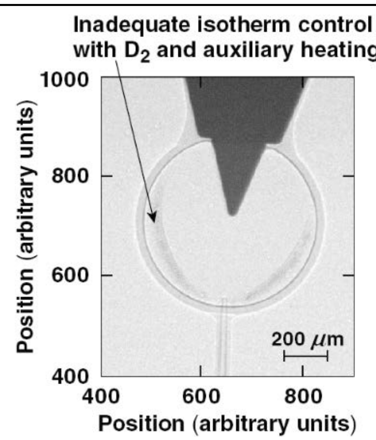

Fig. 30: X-ray phase contrast image showing the D_2 ice formation in a cone-in-shell target. The tip of the cone was heated by an auxiliary laser heating source, which removed the ice from the tip. The target still lacks an adequate isotherm control with D_2 and auxiliary heating. It is expected that with DT the isotherm constraints will be reduced on fuel layering.

3.6. Diagnostic Development

3.6.1. Development of Zr Kα crystal imager

The most widely used diagnostics for laser-generated electron beam studies are spherically bent Bragg crystals used to image laser-generated electrons deep inside dense plasmas. So far, the use of such crystals to select monochromatic radiation from targets has been limited to the spectral range of 1- 10 keV [**Akli10**, Perez10], which limits both the depth at which they can detect and the temperature of plasma that can be used [**Akli07**, Gregori05]. Both are problems when FI targets are doped with a tracer material to study either the implosion symmetry by backlighting or imaging electron beam transport [**Key08**]. We have developed a higher energy Kα imaging diagnostic, a spherically-bent 2354 quartz crystal operating at 15.7 keV, that allows electron imaging from much deeper, hotter plasmas than previously possible [**Akli11**]. The Bragg angle, rocking curve, and reflection efficiency of the quartz crystal were measured at photon energy of 15.6909 keV, corresponding to the $K\alpha_2$ line of Zr, using the X15A beamline at the National Synchrotron Light Source at Brookhaven National Laboratory. One flat and three spherically curved samples were tested. The peak reflectivity of the best-performing crystal was determined to be $(3.6\pm0.7)\times10^{-4}$ with a rocking-curve full width at half maximum of 0.09°. Using one of the curved crystals, the Zr $K\alpha_2$ emission was imaged from a hot Zr plasma generated by the 10-J, Multi-Terawatt laser at LLE. Estimates of the reflectivity obtained by comparing the spatially integrated signal from the images to the direct x-ray emissivity of the source were, within experimental error, in agreement with values obtained at the X15A beamline. This work has been published in the journal of Rev. Sci. Instruments [**Storm13**].

The use of Kα emission in ICF studies is well established, with most applications employing the Kα of Cu at ~8.048 keV. The use of Cu Kα to diagnose the penetration efficiency of fast electrons in hot dense plasmas is limited by the Kα line shift that accompanies high-temperature–induced ionization in the plasma. As the Kα lines shift in energy, they move outside the acceptance bandwidth of the imaging crystals, so, consequently, the detection efficiency drops. The issue of line shifting may be mitigated by using Kα radiation from higher-Z materials, such as Zr, that are more robust against temperature-induced shifts. This hypothesis was tested in an experiment on the Texas PW facility using the Zr Kα crystal imager described above and Zr foil targets of various volumes ranging from 3000 x 3000 x 21 μm^3 to 150 x 150 x 5 μm^3. The overall effect of target heating was significantly mitigated compared to similar size Cu foil targets, although a decrease in efficiency was measured for the smallest volume targets, which experiences the strongest heating.

3.6.2. Time resolved x-ray spectroscopy of high intensity laser driven Al and Si foil targets

The Kα imaging capability on OMEGA and OMEGA EP is being further expanded for fast ignition applications and cryogenic target implosions. The production of ~keV soft x-rays from high intensity, short-pulse laser-plasmas is important for advanced applications like the backlighting of cryogenic targets on OMEGA [**Stoeckl13**]. The physics of short pulse laser-plasma interaction and the coupling of laser energy into both the thermal plasma and into fast electrons were studied in order to optimize the x-ray production from mass limited aluminum foil targets. Foil targets of various sizes from 500 µm down to 20 µm were irradiated with picosecond pulse duration laser pulses at intensities exceeding 10^{19} W/cm^2. The He_α and the Ly_α x-ray line emission was measured spectrally and temporally resolved. In addition, the x-ray source was characterized with a calibrated time-integrated spectrograph. The combination of all those measurements allows one to infer the brilliance of the x-ray line source, which is important information for the back-lighter applications. This work is part of Brian Eichman's thesis work and was presented at the APS DPP conference in 2012 [**Eichman12**].

4. Overall Summary and Impact

Over the whole period of this large collaborative ACE-FI project, we have greatly advanced our understanding of the physical properties in all three thrust areas that affect the characteristics of the LPI and fast electron transport for fast ignition:

- ❖ Fast electron generation through laser-plasma interaction is controlled by the laser intensity distribution and the topology and density gradient near the plasma critical density surface, which co-evolve with laser pulse. Comprehensive studies on fast electron source characteristics (energy conversion, spectrum and divergence) have been performed. Detrimental effects of preplasma (resulting in increased stand-off distances from the source to the high density target as well as large spread of electron beam) have been extensively investigated with detailed physics understanding. *Improved energy coupling have been demonstrated with high contrast lasers extending from sub-ps to FI relevant 10 ps pulses, painting a brighter picture for FI feasibility.*
- ❖ Our detailed experiments and analyses of fast electron transport dependence on target material have shown that it is feasible to collimate fast electron beam by self-generated resistive magnetic fields in engineered targets with a rather simple geometry. Stable and collimated electron beam with spot size as small as 50 μm after > 100 μm propagation distance (a full angular divergence angle of 20°!) in solid density plasma targets has been demonstrated with FI relevant 10 ps laser pulse with kilojoule energies. *Such collimated beam would meet the required heating beam size for FI.*
- ❖ We have developed various transport experiment platforms (from cold to warm dense matter to imploded high density plasmas) and have performed systematic study of fast electron transport and energy deposition in FI relevant condition. Particularly, two new experimental platforms on the OMEGA laser, i.e., i) high resolution 8 keV backlighter platform for cone-in-shell implosion and ii) the 8 keV imaging with doped shell targets for detailed transport characterization, have enabled us to experimentally confirming fuel assembly from cone-in-shell implosion with *record-high areal density as well as the first direct measurement of fast electron transport and spatial energy deposition in integrated FI experiments.*
- ❖ Along the course of the work, new and advanced diagnostics have been implemented and simulations codes with added physics models have been developed/improved and benchmarked against the experiments.

Advances in laser performance, experimental capability, target design, and modeling tools have now provided an unprecedented opportunity for testing sub-ignition-scale cone-in-shell fast-ignition targets and validating large-scale integrated target computer simulations. In addition, our work also has a broad impact to wide range of HED phenomena including high-energy ion beam generation, isochoric heating of materials, and the development of high brightness x-ray sources.

One important aspect of this program was the involvement and training of young scientists including postdoctoral fellows and graduate students. During the entire 8 years of FI and ACE project period since 2005, more than fifteen (15) graduate students directly funded by the ACE program completed their doctoral dissertations including three (3) from OSU and two (2) from UCSD in last three years. Project findings have been presented at various domestic and international conferences and workshops and produced an impressive large number of peer-reviewed publications in high quality journals. A list of five (5) PhD theses and forty (40) journal publications including nine (two under review) in Physical Review Letters since 2011 is given below.

5. PhD Theses and Refereed Journal Publications since 2011

5.1 PhD Theses since 2011

1. Drew P. Higginson, "Ultra-High-Contrast Laser Acceleration of Relativistic Electrons in Solid

Targets", UCSD, 2013.

2. Andrew G. Krygier, "On the Origin of Super-Hot Electrons in Intense Laser-Plasma Interactions", OSU, 2013.
3. George E. Kemp, "Specular Reflectivity and Hot-Electron Generation in High-Contrast Relativistic Laser-Plasma Interactions", OSU, 2013.
4. Bhooshan S. Paradkar, "The effects of pre-formed plasma on the generation and transport of fast electrons in relativistic laser-solid interactions," UCSD, 2012.
5. Vladimir M. Ovchinnikov, "Determining the Properties of Laser Induced Fast Electrons from Experiments and Simulations," OSU, 2011.

5.2 Peer-Reviewed Journal Publication since 2011

1. **D.P. Higginson**, A. Link, H. Sawada, S.C. Wilks, T. Bartal, S. Chawla, C.D. Chen, K.A. Flippo, L.C. Jarrott, M.H. Key, H.S. McLean, P.K. Patel, F. Perez, M.S. Wei, and F.N. Beg, "High-Contrast Laser Acceleration of Relativistic Electrons in Solid Targets", submitted to Phys. Rev. Lett. (2013)
2. **T. Yabuuchi**, J. May, C. McGufey, H. Sawada, M. S. Wei, R. B. Stephens, C. Stoeckl, W. B. Mori, H. S. McLean, P. K. Patel, F. N. Beg, "Reduced fast electron transport in shock-heated plasma due to inhibiting electrostatic fields and self-generated magnetic fields", Submitted to Phys. Rev. Lett. (2013)
3. **S. Chawla**, M. S. Wei, R. Mishra, K.U Akli, C. D. Chen, H. S. McLean, A. Morace, P. K. Patel, H. Sawada, Y. Sentoku, R. B. Stephens, and F.N. Beg, "Effect of target material on fast electron transport and resistive collimation", Phys. Rev. Lett., **110**, 025001 (2013).
4. **V.M. Ovchinnikov**, D.W. Schumacher, M. McMahon, E.A. Chowdhury, C.D. Chen, A. Morace and R.R. Freeman, "Effects of preplasma scale length and laser intensity on the divergence of laser-generated hot electrons," Phys. Rev. Lett., **110**, 065007 (2013).
5. **T. Ma**, H. Sawada, P.K. Patel, C.D. Chen, L. Divol, D.P. Higginson, A. J. Kemp, M. H. Key, D. J. Larson, S. Le Pape, A. Link, A. G. MacPhee, H. S. McLean, Y. Ping, R. B. Stephens, S. C. Wilks, and F. N. Beg, "Hot Electron Temperature and Coupling Efficiency Scaling with Prepulse for Cone-Guided Fast Ignition", Phys. Rev. Lett., **108**, 115004 (2012).
6. **Y. Ping**, A. J. Kemp, L. Divol, M. H. Key, P. K. Patel, K. U. Akli, F. N. Beg, S. Chawla, C. D. Chen, R. R. Freeman, D. Hey, D. P. Higginson, L. C. Jarrott, G. E. Kemp, A. Link, H. S. McLean, H. Sawada, R. B. Stephens, D. Turnbull, B. Westover, and S. C. Wilks, "Dynamics of Relativistic Laser-Plasma Interaction on Solid Targets", Phys. Rev. Lett. **109**, 145006 (2012).
7. **P. M. Nilson**, J. R. Davies, W. Theobald, P. A. Jaanimagi, C. Mileham, R. K. Jungquist, C. Stoeckl, I. A. Begishev, A. A. Solodov, J. F. Myatt, J. D. Zuegel, T. C. Sangster, R. Betti, and D. D. Meyerhofer, "Time-Resolved Measurements of Hot-Electron Equilibration Dynamics in High-Intensity Laser Interactions with Thin-Foil Solid Targets," Phys. Rev. Lett. **108**, 085002 (2012).
8. B. Vauzour, J. J. Santos, A. Debayle, S. Hulin, H.-P. Schlenvoigt, X. Vaisseau, D. Batani, S. D. Baton, J. J. Honrubia, Ph. Nicolai**,** F. N. Beg, R. Benocci, S. Chawla, M. Coury, F. Dorchies, C. Fourment, E. d'Humieres, L. C. Jarrot, P. McKenna, Y. J. Rhee, V. T. Tikhonchuk, L. Volpe, and V. Yahia, "Relativistic High-Current Electron-Beam Stopping-Power Characterization in Solids and Plasmas: Collisional Versus Resistive Effects", Phys. Rev. Lett., **109**, 255002 (2012).
9. F. Perez, A. Debayle, J. Honrubia, M. Koenig, D. Batani, S. D. Baton, F. N. Beg, C. Benedetti, E. Brambrink, S. Chawla, F. Dorchies, C. Fourment, M. Galimberti, L. A. Gizzi, L. Gremillet, R. Heathcote, D. P. Higginson, S. Hulin, R. Jafer, P. Koester, L. Labate, K. L. Lancaster, A. J. MacKinnon, A. G. MacPhee, W. Nazarov, P. Nicolai, J. Pasley, R. Ramis, M. Richetta, J. J. Santos, A. Sgattoni, C. Spindloe, B. Vauzour, T. Vinci, and L. Volpe, "Magnetically Guided Fast Electrons in Cylindrically Compressed Matter", Phys. Rev. Letters, **107**, 065004 (2011).
10. **M. Storm**, B. Eichman, Z. Zhong, W. Theobald, P. Schiebel, C. Mileham, C. Stoeckl, I. A. Begishev, G. Fiksel, R. Stephens, R. R. Freeman, and K. Akli, "Characterization of a High-

Photon Energy X-Ray Imager," Rev. Sci. Instrum. **84**, 106103 (2013).

11. H. Shiraga, H. Nagatomo, W. Theobald, A. A. Solodov, and M. Tabak, "Fast Ignition Integrated Experiments and High-Gain Point Design," submitted to Nuclear Fusion (2013)
12. **J. Li**, J. R. Davies, W. B. Mori, C. Ren, A. A. Solodov, W. Theobald, T. Ma, and J. Tonge, "Hot-Electron Generation from Laser–Pre-Plasma Interactions in Cone-Guided Fast Ignition," Phys. Plasmas **20**, 052706 (2013).
13. **R. Mishra**, P. Leblanc, Y. Sentoku, M. S. Wei, and F. N. Beg, "Collisional particle-in-cell modeling for energy transport accompanied by atomic processes in dense plasmas"**,** Phys. Plasmas **20**, 072704 (2013).
14. **C. D. Chen**, A. J. Kemp, F. Perez, A. Link, F. N. Beg, S. Chawla, M. H. Key, H. McLean, A. Morace, Y. Ping, A. Sorokovikova, R. B. Stephens, M. Streeter, B. Westover, and P. K. Patel, "Comparisons of angularly and spectrally resolved Bremsstrahlung measurements to two-dimensional multi-stage simulations of shor tpulse laser-plasma interactions", Phys. Plasmas **20**, 052703 (2013).
15. **T. Yabuuchi**, R. Mishra, C. McGuffey, B. Qiao, M. S. Wei, H. Sawada, Y. Sentoku, T. Ma, D. P. Higginson, K. U. Akli, D. Batani, H. Chen, L. A. Gizzi, M. H. Key, A. J. Mackinnon, H. S. McLean, P. A. Norreys, P. K. Patel, R. B. Stephens, Y. Ping, W. Theobald, C. Stoeckl, and F. N. Beg, "Impact of extended preplasma on energy coupling in kilojoule energy relativistic laser interaction with cone wire targets relevant to Fast Ignition", New Journal of Physics **15**, 015020 (2013).
16. **G.E. Kemp**, A. Link, Y. Ping, D.W. Schumacher, R.R. Freeman, and Pravesh Patel, "Coupling of laser energy into hot-electrons in high-contrast relativistic laser-plasma interactions," Phys. Plasmas **20**, 033104 (2013).
17. **B. S. Paradkar**, T. Yabuuchi, H. Sawada, D.P. Higginson, A. Link, M. S. Wei, R. B. Stephens, S. I. Krasheninnikov, and F. N. Beg, "Emission of energetic protons from relativistic intensity laser interaction with a cone-wire target", Phys. Rev. E **86**, 056405 (2012).
18. **N. Sinenian**, W. Theobald, J. A. Frenje, C. Stoeckl, F. H. Séguin, C. K. Li, R. D. Petrasso, and R. B. Stephens, "Proton-inferred hot-electron temperatures of cone-in-shell fast-ignition experiments at Omega," Phys. Plasmas **19**, 112708 (2012).
19. **N. Sinenian**, G. Fiksel, J. A. Frenje, C. G. Freeman, M.J.-E. Manuel, D. T. Casey, P. Nilson, C. Stoeckl, W. Theobald, D. D. Meyerhofer, and R. D. Petrasso, "Heavy-ion emission from short-pulse laser-plasma interactions with thin foils," Phys. Plasmas **19**, 093118 (2012).
20. **H. Sawada**, D. P. Higginson, A. Link, T. Ma, S. C. Wilks, H. S. McLean, F. Perez, P. K. Patel and F. N. Beg, "Characterizing the energy distribution of laser-generated relativistic electrons in cone-wire targets", Phys. Plasmas **19**, 103108 (2012).
21. **H. Sawada**, T. Yabuuchi, S.P. Regan, K. Anderson, M.S. Wei, R. Betti, J. Hund, M.H. Key, A.J. Mackinnon, H.S. McLean, R.R. Paguio, P.K. Patel, K.M. Saito, R.B. Stephens, S.C. Wilks, F.N. Beg, "Diagnosing laser-driven, shock-heated foam target with Al absorption spectroscopy on OMEGA EP", High Energy Density Physics **8**,180-183 (2012).
22. **T. Yabuuchi**, H. Sawada, S.P. Regan, K. Anderson, M.S. Wei, R. Betti, J. Hund, M.H. Key, A.J. Mackinnon, H.S. McLean, R.R. Paguio, P.K. Patel, K.M. Saito, R.B. Stephens, S.C. Wilks, and F.N. Beg, "Temporally resolved characterization of shock-heated foam target with Al absorption spectroscopy for fast electron transport study", Phys. Plasmas **19**, 092705 (2012).
23. **B. S. Paradkar**, S. I. Krasheninnikov, and F. N. Beg, "Mechanism of heating of pre-formed plasma electrons in relativistic laser-matter interaction", Phys. Plasmas **19**, 060703 (2012).
24. **K.U. Akli**, C. Orban, D. Schumacher, M. Storm, M. Fatenejad, D. Lamb and R.R. Freeman, Physics Review E (Rapid Communications), "Coupling of high-intensity laser light to fast electrons in cone-guided fast ignition," Phys. Rev. E **86**, 065402(R) (2012).
25. **K. U. Akli**, M. J. Storm, M. McMahon, S. Jiang, V. Ovchinnikov, D. W. Schumacher, R. R. Freeman, G. Dyer, and T. Ditmire, "Time dependence of fast electron beam divergence in ultraintense laser-plasma interactions," Phys. Rev. E **86**, 026404 (2012).

26. **C. Stoeckl**, J. A. Delettrez, R. Epstein, G. Fiksel, D. Guy, M. Hohenberger, R. K. Jungquist, C. Mileham, P. M. Nilson, T. C. Sangster, M. J. Shoup III, and W. Theobald, "Soft X-Ray Backlighting of Direct-Drive Implosions Using a Spherical Crystal Imager on OMEGA," Rev. Sci. Instrum. **83**, 10E501 (2012).
27. D. H. Froula, R. Boni, M. Bedzyk, R. S. Craxton, F. Ehrne, S. Ivancic, R. Jungquist, N. L. Kugland, M. C. Rushford, M. J. Shoup, W. Theobald, and D. Weiner, "Optical diagnostic suite (schlieren, interferometry, and grid image refractometry) on the OMEGA EP using a 10-ps 263-nm probe beam," Rev. Sci. Instrum. **83**, 10E523 (2012).
28. **C. Stoeckl**, G. Fiksel, D. Guy, C. Mileham, P. M. Nilson, T. C. Sangster, M. J. Shoup III, and W. Theobald, "A Spherical Crystal Imager for OMEGA EP," Rev. Sci. Instrum. **83**, 033107 (2012).
29. **H. Sawada**, W. Theobald, C. Stoeckl, G. Fiksel, P. K. Patel, C. D. Chen, T. Yabuuchi, F. N. Beg, R. B. Stephens, K. U. Akli, H. S. McLean and M. H. Key, "Monochromatic Imaging of 8.0 keV Cu K-alpha Emission Induced by Energetic Electrons Generated at OMEGA EP", IEEE Transactions on Plasma, **39**, 2816 - 2817 (2011).
30. **B. Westover**, C. D. Chen, P. K. Patel, M. H. Key, H. McLean, R. Stephens, and F. N. Beg, "Fast Electron Temperature and Conversion Efficiency Measurements in Laser-Irradiated Foil Targets Using a Bremsstrahlung X-Ray Detector," Phys. Plasmas, **18**, 063101 (2011).
31. **W. Theobald**, A. A. Solodov, C. Stoeckl, K. S. Anderson, R. Betti, T. R. Boehly, R. S. Craxton, J. A. Delettrez, C. Dorrer, J. A. Frenje, V. Yu. Glebov, H. Habara, K. A. Tanaka, J. P. Knauer, R. Lauck, F. J. Marshall, K. L. Marshall, D. D. Meyerhofer, P. M. Nilson, P. K. Patel, H. Chen, T. C. Sangster, W. Seka, N. Sinenian, T. Ma, F. N. Beg, E. Giraldez, and R. B. Stephens, "Initial Cone-in-Shell Fast-Ignition Experiments on OMEGA", Phys. Plasmas, **18**, 056305 (2011).
32. **B.S. Paradkar**, M.S. Wei, T. Yabuuchi, R.B. Stephens, S.I. Krasheninnikov and F.N. Beg, "Numerical Modeling of Fast Electron Generation in the Presence of Preformed Plasma in Laser-Matter Interaction at Relativistic Intensities", Phys. Rev. E, **83**, 046401 (2011).
33. **K. U. Akli**, M. Sanchez del Rio, S. Jiang, M. S. Storm, A. Krygier, R. B. Stephens, N. R. Pereira, E. O. Baronova, W. Theobald, Y. Ping, H. S. McLean, P. K. Patel, M. H. Key, and R. R. Freeman, "A novel zirconium Kα imager for high energy density physics research," Rev. Sci. Instrum. **82**, 123503 (2011).
34. **P. M. Nilson**, W. Theobald, C. Mileham, C. Stoeckl, J. F. Myatt, J. A. Delettrez, J. MacFarlane, I. A. Begishev, J. D. Zuegel, R. Betti, T. C. Sangster, and D. D. Meyerhofer, "Target-Heating Effects on the $K_{\square 1,2}$-Emission Spectrum from Solid Targets Heated by Laser-Generated Hot Electrons," Phys. Plasmas **18**, 042702 (2011).
35. **P. M. Nilson**, A. A. Solodov, J. F. Myatt, W. Theobald, P. A. Jaanimagi, L. Gao, C. Stoeckl, R. S. Craxton, J. A. Delettrez, J. D. Zuegel, B. E. Kruschwitz, C. Dorrer, J. H. Kelly, K. U. Akli, P. K. Patel, A. J. MacKinnon, R. Betti, T. C. Sangster, and D. D. Meyerhofer, "Scaling Hot-Electron Generation to Long-Pulse, High-Intensity Lasers–Solid Interactions," Phys. Plasmas **18**, 056703 (2011).
36. **V. M. Ovchinnikov**, D.W. Schumacher, G.E. Kemp, A.G. Krygier, L.D. Van Woerkom, K.U. Akli, R.R. Freeman, R.B. Stephens, A. Link, "Using time-integrated K_α images to study refluxing and the extent of pre-plasmas in LPI experiments," Phys. Plasmas **18**, 112702 (2011).
37. **V. M. Ovchinnikov**, G. E. Kemp, D. W. Schumacher, R. R. Freeman, and L. D. Van Woerkom, "How well do time-integrated Kα images represent hot electron spatial distributions?" Phys. Plasmas **18**, 072704 (2011).
38. **Anthony Link**, Richard R. Freeman, Douglass Schumacher and Linn Van Woerkom, "Effects of target charging and ion emission on the energy spectrum of emitted electrons," Phys. Plasmas **18**, 053107 (2011).
39. **D. W. Schumacher**, G. E. Kemp, A. Link, R. R. Freeman, and L. D. Van Woerkom, "The shaped critical surface in high intensity laser plasma interactions," Phys. Plasmas **18**, 013102 (2011).
40. B. Vauzour, F. Perez, L. Volpe, K. Lancaster, Ph. Nicola, M. Koenig, D. Batani, S.D. Baton, F.N. Beg, C. Benedetti, E. Brambrink, S. Chawla, F. Dorchies, C. Fourment, M. Galimberti, L.A.

Gizzi, R. Heathcote, D.P. Higginson, S. Hulin, R. Jafer, P. Kaoster, L. Labate, A.J. MacKinnon, A.G. MacPhee, W. Nazarov, J. Pasley, C. Regan, X. Ribeyre, M. Richetta, G. Schurtz, A. Sgattoni, and J.J. Santos, "Laser-Driven Cylindrical Compression of Targets for Fast Electron Transport Study in Warm Dense Plasmas," Phys. Plasmas, **18**, 043108 (2011).

6. Bibliography and References Cited

[**Akli07**] K.U. Akli et al., "Temperature sensitivity of Cu Kα imaging efficiency using a spherical Bragg reflecting crystal," *Phys. Plasams* **14**, 023102 (2007).

[**Akli10**] K.U. Akli et al., "A dual channel X-ray spectrometer for fast ignition research," *J. Instrum.* **5**, P07008 (2010).

[**Akli11**] K.U. Akli et al., "A novel zirconium Kα imager for high energy density physics research," *Rev. Sci. Instrum.* **82**, 123503 (2011).

[**Akli12a**] K.U. Akli et al., "Time dependence of fast electron beam divergence in ultraintense laser-plasma interactions", *Phys. Rev. E* **86**, 026404 (2012).

[**Akli12b**] **K.U. Akli** et al., "Coupling of high-intensity laser light to fast electrons in cone-guided fast ignition," Phys. Rev. E **86**, 065402(R) (2012).

[Atzeni09] S. Atzeni, A. Schiavi, and J. R. Davies, "Stopping and scattering of relativistic electron beams in dense plasmas and requirements for fast ignition", *Plasma Phys. Control. Fusion* **51**, 015016 (2009).

[Basov92] N.G. Basov, S.Yu. Gus'kov, and L.P. Feokistov, "Thermonuclear gain of ICF targets with direct heating of ignitor,"*J. Sov. Laser Res.* **13**, 396 (1992).

[**Beg12a**] F.N. Beg, "Fast electron generation and transport in laser-driven shock heated warm dense matter (invited)", *39th European Physical Society Conference on Plasma Physics, 16th International Congress on Plasma Physics, , Stockholm,* Sweden, 2-6 July 2012.

[**Beg12b**] F.N. Beg, "Study of hot electron transport in warm dense plasma using OMEGA EP laser (invited)", *39th IEEE International Conference on Plasma Science*, Edinburgh, Scotland, 8-12 July, 2012

[**Beg13**] F.N. Beg, "Fast Electron Transport and Spatial Energy Desposition in Integrated Fast Ignition Experiments at the Omega Laser Facility (invited)", *8th International Conference on Inertial Fusion Sciences and Applications,* Nara, Japan, 8-13 Sep. 2013

[Chen09] C.D. Chen et al., "Bremsstrahlung and Kα fluorescence measurements for inferring conversion efficiencies into fast ignition relevant hot electrons," *Phys. Plasmas* **16**, 082705 (2009).

[Chen13] C.D. Chen et al., "Comparisons of angularly and spectrally resolved Bremsstrahlung measurements to two-dimensional multi-stage simulations of short-pulse laser-plasma interactions", Phys. Plasmas **20**, 052703 (2013).

[Chrisman08] B. Chrisman et al., "Intensity scaling of hot electron energy coupling in cone-guided fast ignition," *Phys. of Plasmas* **15**, 056309 (2008).

[Debayle10] A. Debayle et al., "Divergence of laser-driven relativistic electron beams," *Phys. Rev. E* **82**, 036405 (2010).

[Desjarlais01] M. P. Desjarlais, "Practical Improvements to the Lee-More Conductivity Near the Metal-Insulator Transition*", Contrib. Plasma Phys* **41**, 267 (2001).

[**Eichman12**] B. Eichman, W. Theobald, et al., "Time-Resolved X-Ray Brightness Measurements from Short-Pulse Laser-Irradiated Thin Foils." 54th Annual Meeting of the APS Division of Plasma Physics, Providence, RI, 29 October–2 November 2012.

[Fonseca02] R. A. Fonseca et al., "OSIRIS: A three-dimensional, fully relativistic particle in cell code for modeling plasma based accelerators," *Lecture Notes in Computer Science* **2331**, 342-351 (2002).

[Fryxell00] B. Fryxell, et al., “FLASH: An Adaptive Mesh Hydrodynamics Code for Modeling Astrophysical Thermonuclear Flashes”, *Astro. J. Supp. Series* **131**, 273 (2000).

[Groom00] D. E. Groom and S. R. Klein, *Eur. Phys. J. C* **15**, 163 (2000).

[Halbleib92] J.A. Halbleib, et al., *IEEE Trans. Nuc. Sci*. **39**, 1025 (1992).

[Hombourger98] C. Hombourger, “An empirical expression for K-shell ionization cross section by electron impact”, *J. Phys. B* **31**, 3693 (1998).

[**Jarrott12**] L.C. Jarrott et al., “Study of Fast Electron Energy Deposition into Imploded High Density Plasma Using Cu-Doped CD Shell Targets”, *54th Annual Meeting of the APS Division of Plasma Physics*, Providence, RI, October 29–November 2, 2012.

[**Jarrott13**] L.C. Jarrott, “Study Of Fast Electron Transport and Spatial Energy Deposition in Imploded Plasmas (invited)”, *International Radiation from High Energy Density Plasmas Workshop*, Lake Tahoe, Nevada, 2-5 April 2013.

[Gregori05] G. Gregori et al., “Experimental characterization of a strongly coupled solid density plasma generated in a short-pulse laser target characterization,”*Contrib. to Plasma Phys.* **3-4**, 284-292 (2005).

[Hatchett00] S.P. Hatchett et al., “Electron, photon, and ion beams from the relativistic interaction of Petawatt laser pulses with solid targets,” *Phys. of Plasmas* **7** 2076-2082 (2000).

[**Higginson10**] D. P. Higginson, “Fast Ignition Relevant Hot Electron coupling at 1 *Bull.*□and 2□,” *Amer. Phys. Soc.,* 52nd Annual Meeting of the APS Division of Plasma Physics , Chicago, Illinois, 8–12 Nov. 2010,

[**Higginson12**] D.P. Higginson, “Experimental and Simulated Coupling and Spectra of Hot Electrons into Cone-Wire Targets (invited)”, *39th IEEE Conference on Plasma Science*, Edinburgh, Scotland, 8-12 July 2012,

[**Higginson13**] D.P. Higginson et al., “High-contrast laser acceleration of relativistic electrons in solid targets”, *Phys. Rev. Lett*. (under review, 2013)

[**Ivancic11**] S. Ivancic, W. Theobald, et al., “Initial Channeling of a Kilojoule-Class Laser in Long-Scale-Length Plasmas,” *53rd Annual Meeting of the APS Division of Plasma Physics*, Salt Lake City, UT, 14–18 November 2011.

[**Ivancic12**] S. Ivancic, W. Theobald, et al., “Ray-Trace Simulations for the Optical 4ω Probe Diagnostic on OMEGA EP,” *54th Annual Meeting of the APS Division of Plasma Physics*, Providence, RI, 29 October–2 November 2012.

[**Ivancic13**] S. Ivancic, W. Theobald, et al., “Optical Probe Measurements of a Plasma Channel for Fast Ignition,” 55th Annual Meeting of the APS Division of Plasma Physics, Denver, Co, 11 November–15 November 2013.

[Kemp08] A.J. Kemp et al., “Hot-electron energy coupling in ultraintense laser-matter interaction,” *Phys. Rev. Lett.* **101**, 075004 (2008).

[Kemp10] A.J. Kemp, B.I. Cohen, and L. Divol, “Integrated kinetic simulation of laser-plasma interactions, fast-electron generation, and transport in fast ignition,” *Phys. Plasmas* **17**, 056702 (2010).

[**Key08**] M.H. Key et al., “Fast ignition relevant study of the flux of high intensity laser-generated electrons via a hollow cone into a laser-imploded plasma,” *Phys. of Plasmas* **15**, 022701 (2008).

[Kodama02] R. Kodama et al., “Fast heating scalable to laser fusion ignition,” *Nature* **418**, 933-934 (2002).

[Lancaster07] K.L. Lancaster et al., “Measurements of energy-transport patterns in petawatt laser-plasma interactions at solid density,” *Phys. Rev. Lett.* **98**, 125002 (2007).

[Larson10] D. Larson et al., “Hybrid simulations for magnetized fast ignition targets and analyzing cone-wire experiments,” Bull. Am. Phys. Soc. **55**, JP9.119 (2010).

[Lee84] Y. T. Lee and R. M. More, "An electron conductivity model for dense plasmas", *Phys. Fluids* **27**, 1273 (1984).

[**LePape08**] S. Le Pape et al., "Density measurement of thick compressed foam using two-dimensional x-ray radiography," *Rev. Sci. Instrum.* **79**, 106104 (2008).

[Li04] C.K. Li and R.D. Petrasso, "Stopping of directed energetic electrons in high-temperature hydrogenic plasmas," *Phys. Rev. E* **70**, 067401 (2004).

[**Link11**] A. Link et al., "Effects of target charging and ion emission on the energy spectrum of emitted electrons," *Phys. Plasmas* **18**, 053107 (2011).

[**Ma12**] T. Ma et al. "Hot Electron temperature and coupling efficiency scaling with prepulse for cone-guided fast ignition, *Phys. Rev. Lett.* **108**, 115004 (2012).

[MacFarlane06] J. J. MacFarlane et al*., High Energy Density Phys.* **3**, 181 (2006)

[**MacPhee10**] A.G. MacPhee et al., "Limitation on prepulse level for cone-guided fast-ignition inertial confinement fusion," *Phys. Rev. Lett.* **104**, 055002 (2010).

[Marinak98] M. M. Marinak et al., "A comparison of three-dimensional multimode hydrodynamic instability growth on various National Ignition Facility capsule designs with HYDRA simulations", *Phys. Plasmas* **5**, 1125 (1998).

[Mishra09] R. Mishra et al., "Hot electron generation forming a steep interface in superintense laser-matter interaction,"*Phys. Plasmas* **16**, 112704 (2009).

[**Mishra13**] R. Mishra et al., "Collisional particle-in-cell modeling for energy transport accompanied by atomic processes in dense plasmas"**,** *Phys. Plasmas* **20**, 072704 (2013).

[Nilson10] P.M. Nilson, "Scaling hot-electron generation to high-power, kilojoule-class laser-solid interactions," *Phys. Rev. Lett.* **105**, 235001 (2010).

[Norreys04] P. A. Norreys et al., "Integrated implosion/heating studies for advanced fast ignition," *Phys. of Plasmas* **11**, 2746-2753 (2004).

[**Ovchinnikov11a**] V.M. Ovchinnikov et al., "How well do time-integrated Kα images represent hot electron spatial distributions," *Phys. Plasmas* **18**, 072704 (2011).

[**Ovchinnikov11b**] V.M. Ovchinnikov et al., "Using time-integrated Kα images to study refluxing and the extent of pre-plasmas in LPI experiments," *Phys. Plasmas*. **18**, 112702 (2011).

[**Ovchinnikov13**] V.M. Ovchinnikov et al., "Effects of preplasma scale length and laser intensity on the divergence of laser-generated hot electrons,", *Phys. Rev. Lett.* **110**, 065007 (2013).

[**Paradkar11**] B.S. Paradkar et al., "Numerical modeling of fast electron generation in the presence of preformed plasma in laser-matter interaction at relativistic intensities," *Phys. Rev. E* **83**, 046401 (2011).

[**Peebles13**] J. Peebles et al., "Study of Pre-Plasma Effects on Fast Electron Generation and Transport using the 1.5 kJ, 10 ps OMEGA EP Laser with Bremsstrahlung Spectrometers", *Stewardship Science Academic Program Annual Review Symposium*, Albuquerque, NM, 27-28 June 2013.

[Perez10] F. Perez et al., "Enhanced isochoric heating from fast electrons produced by high-contrast, relativistic-intensity laser pulses," *Phys. Rev. Lett.* **104**, 085001 (2010).

[Prism] Prism Computational Sciences, Madison WI 53711

[**Qiao13**] B. Qiao et al., "Fast electron generation and transport from ten-picosecond laser-plasma interactions in the cone-guided fast ignition", to be presented at the 55th Annual Meeting of the APS Division of Plasma Physics, Denver, CO, 11-15 Nov. 2013.

[Radha05] P. B. Radha et al., "Multidimensional analysis of direct-drive, plastic-shell implosions on OMEGA," *Phys. Plasmas* **12**, 056307 (2005).

[Robinson07] A.P.L. Robinson and M. Sherlock, "Magnetic collimation of fast electrons produced by ultraintense laser irradiation by structuring the target composition", *Phys. Plasmas* **14**, 083105 (2007).

[**Sawada12**] H. Sawada et al., "Diagnosing Laser-Driven, Shock-Heated Foam Target with Al Absorptio Spectroscopy on OMEGA EP," *High Energy Density Phys*. **8**, 180 (2012).

[Sentoku08] Y. Sentoku, A.J. Kemp, "Numerical methods for particle simulations at extreme densities and temperatures: Weighted particles, relativistic collisions and reduced currents," *J. Comp. Phys.* **227**, 6846 (2008).

[Solodov09] A.A. Solodov et al., "Integrated simulations of implosion, electron transport, and heating for direct-drive fast-ignition targets," *Phys. Plasmas* **16**, 056309 (2009).

[Sorokovikova12] A. Sorokovikova et al., "Investigation of high-intensity laser-plasma interaction and fast electron source characteristics from 1-10 ps pulse length", *54th Annual Meeting of the APS Division of Plasma Physics,* , Providence, RI, October 29–November 2, 2012.

[Sorokovikova13] A. Sorokovikova, B. Qiao et al., "Intense laser-plasma interaction and fast electron generation in multi-picosecond time scales", To be submitted to *Phys. Plasmas* (2013).

[Stephens04] R.B. Stephens et al., "K□ fluorescence measurement of relativistic electron transport in the context of fast ignition," *Phys Rev E* **69**, 066414 (2004).

[**Stoeckl12a**] C. Stoeckl et al., "A spherical crystal imager for OMEGA EP," *Rev. Sci. Instrum*. **83**, 033107 (2012).

[**Stoeckl12b**] C. Stoeckl et al., "Soft x-ray backlighting of direct-drive implosions using a spherical crystal imager on OMEGA," *Rev. Sci. Instrum*. **83,** 10E501 (2012).

[**Stoeckl13**] C. Stoeckl et al., "Soft X-ray Backlighting of Cryogenic Implosions Using a Narrowband Crystal Imaging System." 55th Annual Meeting of the APS Division of Plasma Physics, Denver, Co, 11 November–15 November 2013.

[Storm13] M. Storm, B. Eichman, Z. Zhong, W. Theobald, P. Schiebel, C. Mileham, C. Stoeckl, I. A. Begishev, G. Fiksel, R. Stephens, R. R. Freeman, and K. Akli, "Characterization of a High-Photon Energy X-Ray Imager," Rev. Sci. Instrum. **84**, 106103 (2013).

[Tabak94] M. Tabak et al., "Ignition and high gain with ultrapowerful lasers," *Phys. Plasmas* **1** 1626-1634 (1994).

[Theobald09] W. Theobald et al., "Advanced-ignition-concept exploration on OMEGA," *Plasma Phys. Control. Fusion* **51**, 124052 (2009).

[Theobald11] W. Theobald et al., "Initial cone-in-shell fast-ignition experiments on OMEGA," *Phys. Plasmas* **18**, 056305 (2011).

[**Theobald12**] W. Theobald et al., "Monochromatic 8.05-keV Flash Radiography of Imploded Cone-in-Shell Targets." 54th Annual Meeting of the APS Division of Plasma Physics, Providence, RI, 29 October–2 November 2012.

[**Wei10**] M.S. Wei, "Study of fast electron source and transport in laser-driven shock heated warm dense matter (invited)," 53rd Amer. Phys. Soc. – Div. Plasma Phys., Chicago, IL 8-12 November 2010.

[Wei11] M.S. Wei et al., "Dependence of energy coupling on target material and preplasma," presented at the *7th Int. Conf. on Inertial Fus. Sci. & Applic.*, , Bordeaux-Lac, France, 12-16 Sept. 2011.

[Wei12] M.S. Wei et al., "Study of Fast Electron Generation and Transport for Fast Ignition (invited)," *24th IAEA Fusion Energy Conference*, San Diego, CA, 8-13 Oct. 2012.

[Wei13a] M.S. Wei et al., "Effects of target material on fast electron transport and resistive collimation (from Titan to OMEGA EP) (invited)," *NIF & JLF User Group Workshop*, Livermore, CA, 10 -13 Feb. 2013.

[Wei13b] M.S. Wei et al., **"**Dependence of Fast-Electron Generation and Transport on Laser Pulse Length and Preplasma Using OMEGA EP Laser", *Stewardship Science Academic Program Annual Review Symposium*, Albuquerque, NM, 27-28 June 2013.

[**Wei13c**] M.S. Wei et al., "Fast electron transport in laser driven shock heated high density foam plasmas" submitted to *Phys Rev. Lett. (under revision, 2013)*

[Welch06] D.R. Welch et al., "Integrated simulation of the generation and transport of proton beams from laser-target interaction", *Phys. Plasmas* **13**, 063105 (2006).

[Westover11] B. Westover et al., "Fast electron temperature and conversion efficiency measurements in laser-irradiated foil targets using a bremsstrahlung x-ray detector," *Phys. Plasmas* **18**, 063101 (2011).

[Wilks92] S.C. Wilks et al., "Absorption of ultra-intense laser pulses," *Phys. Rev. Lett.* **69** 1383-1386 (1992).

[**Yabuuchi11**] T. Yabuuchi, "Study of fast electron transport in plasmas using a kJ-class laser pulse (Invited)," 12th Int. Workshop on Fast Ignition of Fus. Targets, Bordeaux-Lac, France, 12-16 September 2011.

[**Yabuuchi12**] T. Yabuuchi et al., "Temporally resolved characterization of shock-heated foam target with Al absorption spectroscopy for fast electron transport study", Phys. Plasmas **19**, 092705 (2012)

[**Yabuuchi13a**] T. Yabuuchi, R. Mishra et al., "Impact of extended preplasma on energy coupling in kilojoule energy relativistic laser interaction with cone wire targets relevant to fast ignition", *New Journal of Physics,* **15,** 015020 (2013).

[**Yabuuchi13b**] T. Yabuuchi, J. May et al., "Reduced fast electron transport in shock-heated plasma due to inhibiting electrostatic fields and self-generated magnetic fields", Submitted to Phys. Rev. Lett. (2013)